

PLANETARY NEBULAE AS STANDARD CANDLES. V. THE DISTANCE TO THE VIRGO CLUSTER

GEORGE H. JACOBY¹ AND ROBIN CIARDULLO¹

Kitt Peak National Observatory, National Optical Astronomy Observatories

AND

HOLLAND C. FORD²

The Johns Hopkins University and Space Telescope Science Institute

Received 1989 October 11; accepted 1989 December 20

ABSTRACT

We identify and measure the [O III] $\lambda 5007$ fluxes of 486 planetary nebula candidates in six early-type galaxies (NGC 4374, 4382, 4406, 4472, 4486, and 4649) in the core of the Virgo Cluster. Following the procedures and calibrations outlined in previous papers in this series, we compare the observed planetary nebula luminosity functions to an empirical model based on the planetary nebulae in M31 and derive distances to the galaxies of 15.7, 14.4, 15.7, 13.9, 14.5, and 14.2 Mpc. These distances exhibit superb agreement with a dispersion of only 0.8 Mpc and suggest that the cluster depth is less than 2 Mpc. Most importantly, the distances are totally uncorrelated with parent galaxy metallicity, color, UV flux, or Hubble type.

After accounting for all contributions to the uncertainty, we derive a mean distance of 14.7 ± 1.0 Mpc to the core of the Virgo Cluster. This distance implies that the Hubble constant falls in the range of 81 ± 6 to 94 ± 6 km s⁻¹ Mpc⁻¹, depending on the adopted Virgo velocity and infall model.

Subject headings: cosmology — galaxies: clustering — galaxies: distances — nebulae: planetary

I. INTRODUCTION

Beginning with the pioneering studies by Shapley and Ames (1926), the Virgo Cluster has played a critical role in extragalactic studies. The cluster is sufficiently distant to take part in the Hubble expansion, yet near enough for astronomers to apply a variety of distance indicators to its wide range of galaxy types.

Unfortunately, during the period since Hubble and Humason (1931) published their estimate for the distance to the Virgo Cluster (1.8 Mpc), an unabated controversy has surrounded all attempts to define this distance accurately. Remarkably, virtually every result can be classified as either a “short” (12–16 Mpc) or a “long” (20–24 Mpc) distance, and the uncertainties estimated by various authors rarely overlap both groups. The principal investigators favoring the shorter distance scales are de Vaucouleurs (1985), Aaronson *et al.* (1986), and Pierce and Tully (1988), while the foremost investigators promoting the longer distance scales are Sandage and Tammann (1984). Significant contributions have also been made, for example, by Bottinelli *et al.* (1986), Pritchett and van den Bergh (1987), and Harris (1988). Excellent reviews discussing this topic are available by Rowan-Robinson (1988), Tammann (1988), and van den Bergh (1989).

Why does the debate persist, despite nearly 60 years of technological improvements? No simple answer will do, but a primary contributor must be that at the distance of Virgo the most unassailable extragalactic distance indicators (RR Lyrae and Cepheid variables) are beyond the reach of current instru-

ments and telescopes (see the discussion in Sandage and Tammann 1981a). Therefore, if the issue is to be resolved without resorting to future technology, a new and reliable distance indicator must be defined.

Planetary nebulae (PN) appear to be just such a distance indicator. In Papers I–IV (Jacoby 1989; Ciardullo *et al.* 1989; Jacoby *et al.* 1989; Ciardullo, Jacoby, and Ford 1989) we presented the physical rationale for using the planetary nebula luminosity function (PNLF) to derive extragalactic distances with high accuracy, and we demonstrated how to calibrate, test, and apply the method.

In the specific case of the Virgo Cluster, the PNLF technique offers numerous advantages over other distance estimators.

1. PN are found in all Hubble types and are especially easy to identify in early-type galaxies such as those which best define the Virgo core. Distance measurements to late-type galaxies must be interpreted in the context of their spatial relationship to the cluster center when deriving the distance to the “Virgo Cluster” (van den Bergh 1989). Furthermore, those indicators which are applied to late-type galaxies (e.g., H I line width relations, Cepheids) invariably must be corrected for the effect of dust internal to the galaxy and are therefore subject to an additional uncertainty.

2. PN observations are needed only once, in contrast to the multiple observation epochs required by the variable star standard candles.

3. The PNLF signature is a very sharp cutoff at the bright end, extending over only 0.8 mag (Paper I). This is much more favorable than those methods which use the globular cluster luminosity function where the peak must be identified at roughly 3 mag below the brightest cluster.

4. The PN identification technique utilizes imaging through narrow-band filters which are highly effective at reducing the background contamination from the parent galaxy and from field stars. The subsequent photometric reductions can be per-

¹ Visiting Astronomer, Canada-France-Hawaii Telescope, operated by the National Research Council of Canada, the Centre National de la Recherche Scientifique de France, and the University of Hawaii.

² Visiting Astronomer, Kitt Peak National Observatory, operated by the Association of Universities for Research in Astronomy, Inc., under cooperative agreement with the National Science Foundation.

TABLE 1
OBSERVED PROPERTIES OF PROGRAM GALAXIES

Galaxy	Messier Number	Hubble ^a Type	B^a	Velocity ^a (km s ⁻¹)	Θ^b	[Fe/H] ^c	($B-V$)	($m_{1550} - V$) ^d
NGC 4374.....	M84	E1	10.23	952	1 ^o 31	0.29	0.97 ^e	3.55
NGC 4382.....	M85	SO ₁	10.10	739	5 ^o 66	...	0.90 ^f	4.22
NGC 4406.....	M86	SO ₁ /E3	10.02	-250	1 ^o 05	0.31	0.98 ^e	3.72
NGC 4472.....	M49	E1/SO ₁	9.32	961	4 ^o 66	0.29	1.00 ^e	3.42
NGC 4486.....	M87	E0	9.62	1254	0 ^o 29	0.23	0.99 ^f	2.04
NGC 4649.....	M60	SO ₁	9.83	1259	3 ^o 44	0.42	1.02 ^e	2.24

^a From the RSA catalog; Sandage and Tammann 1981b.

^b Angular distance from cluster center defined by Huchra 1985.

^c Metallicity computed using the Mg₂ measurements of Davies *et al.* (1987) as calibrated by Terlevich *et al.* 1981.

^d From Burstein *et al.* 1988.

^e From Poulain 1988.

^f From Michard 1982.

formed in uncrowded fields and suffer from fewer analysis uncertainties than do methods relying on deep broad-band imaging. In addition, the PN targets have completely stellar point spread functions, further easing the analysis burden.

5. The PN population is derived from a similar stellar population in all early-type galaxies. Thus, the PNLf should be subject only to effects of metallicity variations, if any. We have shown in Paper IV that the PNLfs for three galaxies in the Leo Cloud are indistinguishable, and the data presented in this paper provide much stronger evidence that this indeed is the case.

The primary disadvantages of using the PNLf are that (1) the calibration requires that PN be secondary indicators, and (2) the best calibrator (M31) is of a later type than the galaxies in this study. Regarding the first issue, Paper III showed that the PN distance estimate to M81 is in excellent agreement with the distance derived from *I*-band observations of Cepheids, indicating that the accuracy of the PNLf method is at least as good as that using Cepheids. As for the latter issue, Paper IV demonstrated that the PNLf yields identical results for three galaxies with similar distances but different Hubble types (though none was as late as M31). We will discuss this further in §§ IV and V.

In this paper, the fifth of the series, we apply the PNLf method to six galaxies in the core of the Virgo Cluster. In § II, we discuss our galaxy selection criteria and describe the observations. In § III, we present the identifications and coordinates of 486 PN candidates in the six galaxies and present the details of our photometric reductions. In § IV we define statistically homogeneous samples of PN and explain how we use these data to derive distances and formal errors. In § V we compare our results with those derived from other methods and review the issue of metallicity effects on derived distances. We conclude by discussing the implications that our distance has on the Hubble constant.

II. OBSERVATIONS

a) Galaxy and Field Selection

The distance that one derives to the "Virgo Cluster" depends to some degree on the choice of the galaxies used to define the cluster. Selecting all late-type galaxies would lead to an anomalous result if a significant fraction of these galaxies were subclustered at a distance other than that of the main body of the cluster. Evidence for exactly this phenomenon has been presented by de Vaucouleurs (1961), Huchra (1985),

Binggeli, Tammann, and Sandage (1987), and Pierce and Tully (1988), among others. It appears, in fact, that the core of the cluster is best defined by the early-type galaxies (van den Bergh 1989).

We chose six of the dominant early-type galaxies in the 6^o core as our initial sampling of the distance to Virgo. Our selection criteria were (1) the galaxies had to be bright ($V < 12$) so that we could expect to identify a sufficient number of PN in their halos, (2) the galaxies had to have velocities less than 1500 km s⁻¹ in order to have the emission line of [O III] λ 5007 fall within the bandpass of our narrow-band filters, and (3) the galaxies had to have diameter-velocity dispersion distance estimates (Faber *et al.* 1989) suggesting membership in the cluster. In addition, some preference was given to galaxies with extreme values of metallicity (Davies *et al.* 1987) or UV color (Burstein *et al.* 1988) so that any systematic effects in the PNLf would be more evident. A summary of the galaxies selected and their properties is listed in Table 1.

It is difficult to detect PN close to the nucleus of a galaxy due to the high background surface brightness. At the same time, however, a single CCD field in the halo is generally too small to identify a sufficient number of PN candidates for an accurate determination of the PNLf. Consequently, we attempted to observe two fields per galaxy, each offset 1'–2' from the galaxy nucleus. The coordinates of the selected field centers are given in Table 2, and the fields surveyed are illustrated in Figure 1.

b) The Data

We identify PN in distant galaxies using the on-band/off-band technique described in Papers II, III, and IV. Briefly, we

TABLE 2
CENTERS OF PLANETARY NEBULAE SURVEY FIELDS

Galaxy	$\alpha(1950)$	$\delta(1950)$
NGC 4374 Field 1	12 ^h 22 ^m 23 ^s .9	13 ^o 09'45"
NGC 4374 Field 2	12 22 38.8	13 09 44
NGC 4382	12 22 52.0	18 26 13
NGC 4406 Field 1	12 23 47.7	13 12 43
NGC 4406 Field 2	12 23 32.0	13 14 01
NGC 4472 Field 1	12 27 13.0	8 17 54
NGC 4472 Field 2	12 27 15.3	8 15 09
NGC 4486 Field 1	12 28 17.2	12 37 27
NGC 4486 Field 2	12 28 17.9	12 41 11
NGC 4649	12 41 08.8	11 47 46

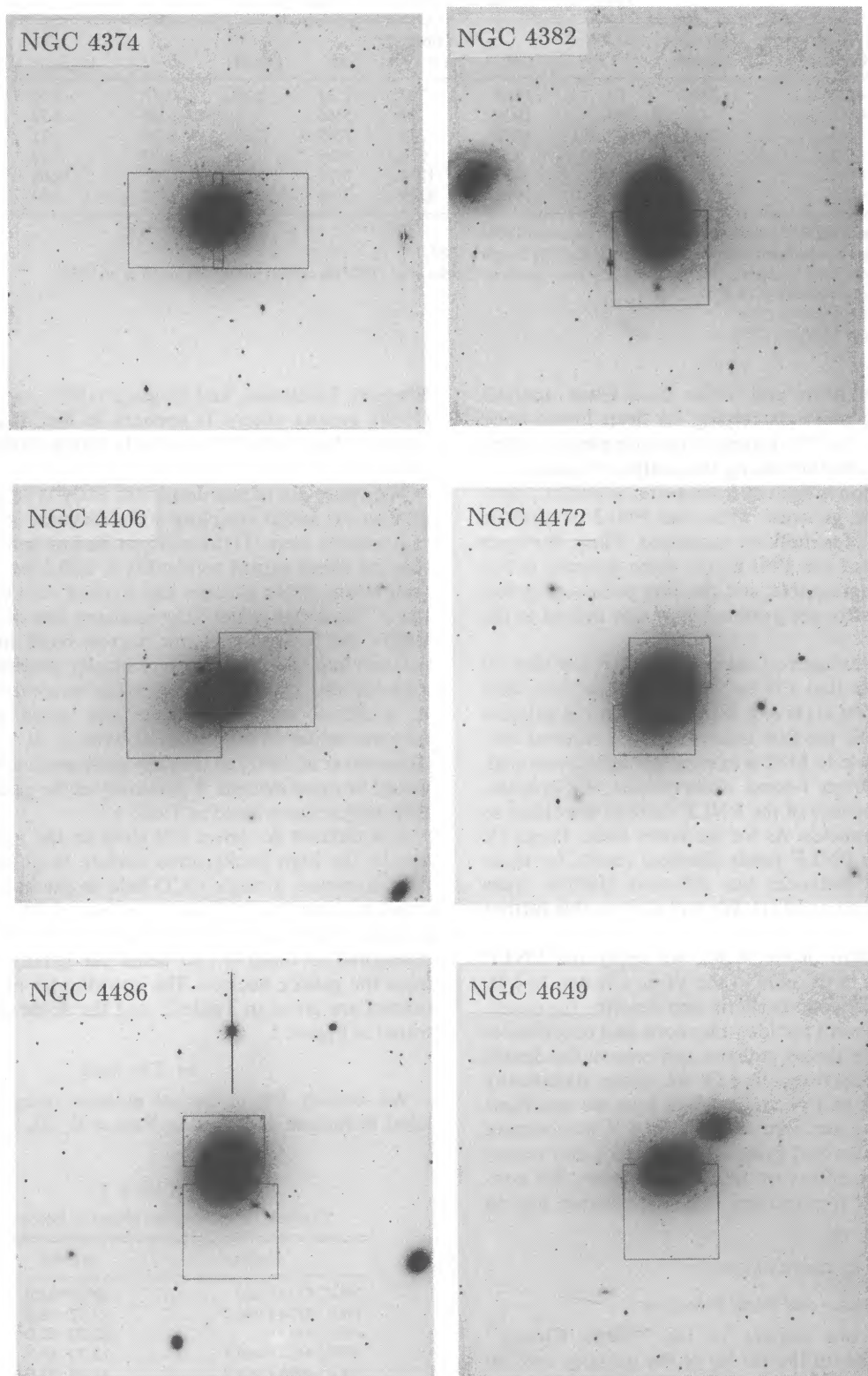


FIG. 1.—The survey fields are shown overlaid on the wide-field ($18' \times 18'$) Tektronix 2048×2048 images of the six Virgo galaxies. The rectangular fields ($2.2 \times 3.5'$) were obtained at the CFHT, and the square fields ($4' \times 4'$) were obtained at the Kitt Peak 4 m telescope. North is at the top and east is to the left.

obtain a series of [O III] $\lambda 5007$ images of each galaxy field through a narrow-band filter having a central wavelength shifted to the systemic velocity of the parent galaxy. A corresponding set of images is then taken through an intermediate bandpass filter centered near $\lambda 5300$. Typical full width at half-maximum (FWHM) values for these filters are 30 \AA and 275 \AA , respectively. PN candidates are found according to their presence in the on-band frame and absence in the off-band frame (see § IIIa).

A feasibility test was made in one field of M87 in 1985 April at the Kitt Peak 4 m telescope (KPNO) using the TI2 CCD in 2×2 on-chip summation mode ($0''.60$ per pixel). The remaining data were obtained in 1989 March at the Canada-France-Hawaii telescope (CFHT) using the RCA2 CCD in 2×2 on-chip summation mode ($0''.41$ per pixel) and in 1989 April at KPNO, again using the 4 m and TI2 CCD, but in the default ($0''.30$ per pixel) mode. Seeing was typically about $1''.4$ during the feasibility test in 1985, $0''.8$ at CFHT, and $1''.0$ at KPNO in 1989. In all, four different on-band filters were required to observe the six galaxies. This large number of filters was due, in part, to the range in systemic velocities, and due also to the two different telescope f-ratios (see Paper III). We summarize the observational parameters in Table 3.

In addition to the aforementioned data which were used to identify PN candidates and measure their brightnesses, we also obtained a 15 minute broad-band V image of each galaxy with a Tektronix 2048×2048 CCD at KPNO. These large-format frames ($18'$ on a side; see Fig. 1) were used to define an astrometric grid of stars in the smaller fields of the CFHT RCA2 and KPNO TI2 CCDs. Finally, for those galaxies in which we obtained data in two fields, we also took [O III] narrow-band images centered on the galaxy nucleus in order to tie the fields onto a common photometric system (cf. Ciardullo *et al.* 1987). These additional observations are also listed in Table 3.

In order to transform from the narrow-band instrumental magnitudes to an absolute flux scale, we observed typically four of the following spectrophotometric standard stars each night: BD +8 2015, BD +25 3941, BD +33 2642, BD +40 4032, Feige 34, Feige 56, Feige 92, He 3, and Kopff 27 (Stone 1977; Oke 1974).

III. REDUCTIONS

a) Identification of the Planetary Nebula Candidates

We followed the procedures for identifying PN candidates as described in Papers II, III, and IV. We began by spatially registering all the individual frames of each field using 5 to 10 stars to define the coordinate system. The on-band [O III] $\lambda 5007$ frames were then averaged together, as were the off-band

$\lambda 5300$ frames. We then "blinked" the on-band grand average against the off-band grand average, noting those stellar objects which were clearly visible on the on-band frame, but absent on the off-band frame.

To guard against confusion with cosmic rays and other spurious detector anomalies which are common during long exposures, we also split the on-band frames into two independent subgroups. We then examined the image of each PN candidate on both subgroups for the signature of a false detection. A typical cosmic-ray event, for example, was bright in one subgroup, but absent in the other. Only for the very faintest candidates was there any confusion; the brighter candidates were visible on each of the contributing frames.

A test we performed later in the reduction phase, the comparison of the radial distribution of PN candidates with the galaxy's luminosity profile, confirmed that contamination is unimportant. In all cases, the candidates follow the distribution of galaxy light quite well, a property of PN seen in M31 (Paper II), M81, (Paper III), and the Leo Group galaxies (Paper IV). If the list of candidates contained a significant number of false detections, this correlation would have been inverted; that is, since cosmic rays and detector radiation events, which fall across the chip randomly, are more difficult to see against the brighter parts of the galaxy, an anti-correlation with galaxy light would have been found.

After excluding the anomalous detector events, 486 PN candidates remained in the six galaxies. Lists of these are presented in Tables 4–9.

b) Astrometry

Accurate coordinates for the PN serve two purposes. First, as noted above, it is useful to test how well the PN follow the distribution of light in a galaxy. Because this test requires knowing the location of a galaxy's nucleus (which was not always included in our survey fields), we need a way to place all positions (PN and galaxy nucleus) on a common astrometric system. Standard right ascension and declination provide such a system. The second purpose relates to the future use of halo PN in kinematic studies which will probe for the presence of dark matter.

Our CCD survey fields were far too small to contain enough coordinate reference stars and, in fact, such stars are usually so bright that they must be avoided during any deep survey. Consequently, we had to define a series of secondary positional standard stars. Again, we attempted to follow the procedures outlined in Papers III and IV where Palomar Observatory Sky Survey (POSS) plates or wide field plates borrowed from the KPNO archives were used to derive the positions of secondary

TABLE 3
SUMMARY OF OBSERVATIONS

Galaxy	Telescope	Detector	Filter ^a λ_c /FWHM	Date	Number of fields	Exposure (hours)	Seeing	Tie-In Exposure (hours)
NGC 4374.....	KPNO 4 m	TI2	5023/31	1989 Apr	2	8	$1''.2$	0.17
NGC 4382.....	KPNO 4 m	TI2	5023/31	1989 Apr	1	4	$0''.8$...
NGC 4406.....	KPNO 4 m	TI2	4998/30	1989 Apr	2	6	$1''.0$	0.33
NGC 4472.....	CFHT	RCA2 ^b	5028/30	1989 Mar	2	8	$0''.8$	0.50
NGC 4486.....	{ KPNO 4 m	TI2 ^b	5022/30	1985 Apr	1	6	$1''.4$	0.25
		CFHT	RCA2 ^b	5028/30	1989 Mar	1	3	$0''.8$
NGC 4649.....	KPNO 4 m	TI2	5027/33	1989 Apr	1	5.5	$1''.6$...

^a Filter characteristics given at observing temperature and telescope f/ratio ($f/2.7$ for KPNO 4 m; $f/4.2$ for CFHT).

^b Detector used in 2×2 on-chip summation mode.

TABLE 4
 NGC 4374 PLANETARY NEBULAE

ID	$\alpha(1950)$	$\delta(1950)$	m_{5007}	Sample	ID	$\alpha(1950)$	$\delta(1950)$	m_{5007}	Sample
1	12 22 42.77	13 09 48.3	26.24		52	12 22 24.60	13 10 56.4	27.22	S
2	12 22 31.21	13 10 52.1	26.39		53	12 22 19.53	13 09 03.3	27.22	S
3	12 22 45.52	13 11 31.3	26.39	S	54	12 22 36.79	13 10 42.7	27.22	
4	12 22 30.96	13 11 00.4	26.58		55	12 22 46.00	13 09 03.4	27.22	S
5	12 22 33.06	13 10 50.2	26.61		56	12 22 35.92	13 10 33.4	27.25	
6	12 22 34.39	13 10 09.8	26.61		57	12 22 44.08	13 08 00.8	27.27	S
7	12 22 18.57	13 09 51.7	26.62	S	58	12 22 29.82	13 11 25.2	27.29	
8	12 22 35.84	13 10 29.1	26.64		59	12 22 35.69	13 09 16.5	27.30	
9	12 22 25.91	13 11 22.2	26.66	S	60	12 22 36.98	13 07 55.3	27.31	
10	12 22 18.24	13 11 30.0	26.70	S	61	12 22 28.21	13 10 59.5	27.31	
11	12 22 30.98	13 11 00.6	26.71		62	12 22 31.10	13 08 37.5	27.32	
12	12 22 39.52	13 09 15.8	26.73	S	63	12 22 27.59	13 10 48.0	27.33	
13	12 22 35.23	13 11 38.7	26.73	S	64	12 22 28.56	13 07 59.5	27.33	
14	12 22 42.46	13 09 48.5	26.75	S	65	12 22 39.45	13 10 14.9	27.33	
15	12 22 33.86	13 10 46.2	26.77		66	12 22 27.02	13 08 52.0	27.34	
16	12 22 26.41	13 11 28.6	26.81	S	67	12 22 26.36	13 09 20.4	27.35	
17	12 22 23.67	13 10 08.6	26.81	S	68	12 22 44.64	13 10 45.3	27.35	
18	12 22 45.15	13 11 08.5	26.84	S	69	12 22 23.72	13 08 29.5	27.37	
19	12 22 40.65	13 10 10.9	26.85	S	70	12 22 31.36	13 11 36.7	27.39	
20	12 22 22.70	13 11 23.2	26.85	S	71	12 22 34.86	13 10 41.6	27.43	
21	12 22 36.29	13 08 56.6	26.89		72	12 22 23.02	13 08 48.6	27.43	
22	12 22 34.57	13 11 28.7	26.91	S	73	12 22 38.00	13 10 44.3	27.44	
23	12 22 24.13	13 08 00.6	26.92	S	74	12 22 36.76	13 08 59.1	27.47	
24	12 22 25.54	13 10 29.4	26.92		75	12 22 29.55	13 08 49.9	27.48	
25	12 22 34.57	13 09 27.7	26.94		76	12 22 37.49	13 09 36.0	27.50	
26	12 22 35.89	13 09 09.1	26.94		77	12 22 46.17	13 09 29.0	27.51	
27	12 22 38.23	13 10 34.9	26.95	S	78	12 22 29.23	13 08 11.3	27.51	
28	12 22 34.76	13 09 27.7	26.95		79	12 22 29.38	13 08 11.4	27.54	
29	12 22 28.29	13 11 22.0	26.95	S	80	12 22 22.90	13 10 25.6	27.58	
30	12 22 21.15	13 11 05.1	26.98	S	81	12 22 46.37	13 09 30.7	27.62	
31	12 22 36.74	13 11 19.2	27.01	S	82	12 22 36.15	13 09 21.1	27.63	
32	12 22 22.93	13 11 22.6	27.02	S	83	12 22 32.64	13 11 06.0	27.63	
33	12 22 39.12	13 08 26.5	27.02	S	84	12 22 38.81	13 08 58.6	27.70	
34	12 22 20.46	13 09 58.3	27.04	S	85	12 22 23.52	13 09 50.8	27.74	
35	12 22 23.81	13 11 36.3	27.06	S	86	12 22 38.96	13 08 42.2	27.78	
36	12 22 41.80	13 10 51.3	27.06	S	87	12 22 20.32	13 10 32.1	27.83	
37	12 22 29.11	13 07 56.2	27.06	S	88	12 22 27.19	13 11 24.4	27.85	
38	12 22 31.79	13 08 31.0	27.07		89	12 22 18.11	13 10 49.9	27.88	
39	12 22 31.72	13 11 10.3	27.10		90	12 22 22.29	13 09 48.3	27.94	
40	12 22 38.71	13 11 12.1	27.10	S	91	12 22 26.16	13 08 43.1	27.95	
41	12 22 22.43	13 09 16.5	27.11	S	92	12 22 26.55	13 08 21.2	27.96	
42	12 22 42.06	13 10 56.8	27.13	S	93	12 22 45.98	13 09 13.2	28.00	
43	12 22 37.89	13 09 53.1	27.13		94	12 22 39.19	13 11 03.5	28.06	
44	12 22 39.33	13 09 37.9	27.13	S	95	12 22 45.54	13 08 24.6	28.08	
45	12 22 23.85	13 10 08.8	27.14	S	96	12 22 39.16	13 11 12.6	28.09	
46	12 22 37.28	13 09 39.6	27.16		97	12 22 37.54	13 08 48.8	28.11	
47	12 22 21.18	13 07 59.1	27.17	S	98	12 22 30.08	13 11 19.4	28.16	
48	12 22 31.82	13 08 31.2	27.17		99	12 22 27.29	13 11 25.7	28.18	
49	12 22 37.77	13 08 47.6	27.18	S	100	12 22 41.47	13 09 48.6	28.24	
50	12 22 28.09	13 08 13.9	27.19	S	101	12 22 23.69	13 10 16.8	28.25	
51	12 22 19.60	13 09 41.0	27.21	S	102	12 22 22.76	13 11 10.3	28.36	

standard stars which fell in the CCD survey fields. For many of the Virgo fields, however, there were too few stars visible on the POSS to define the coordinate system adequately, and deep wide field plates of most of our program galaxies were unavailable.

Our astrometric measurements therefore required a three-step process. First, the POSS was used to define a sequence of ~ 15 secondary standard stars which were contained on the Tektronix 2048 \times 2048 CCD image of each galaxy. These stars were then used to define a tertiary sequence of 8–10 fainter stars contained in each of the PN survey fields. These stars (actually globular clusters in many cases) provided the final

astrometric calibration. Tables 4–9 list the PN coordinates. The coordinates of the brightest tertiary standard stars are presented in Table 10. Despite the complexity of the procedure, we estimate the uncertainty in the PN positions to be less than 1"; the high quality of the Tektronix CCD data produced very accurate transformations.

c) Photometry

In Papers III and IV we described the technique of differencing on-band and off-band images to help identify PN candidates and remove the rapidly varying background of the underlying galaxy. This procedure has several advantages: the

TABLE 5
NGC 4382 PLANETARY NEBULAE

ID	$\alpha(1950)$	$\delta(1950)$	m_{5007}	Sample	ID	$\alpha(1950)$	$\delta(1950)$	m_{5007}	Sample
1	12 22 47.94	18 25 18.6	25.21		52	12 22 43.90	18 27 05.8	27.07	S
2	12 22 55.94	18 27 53.7	26.22	S	53	12 22 52.36	18 25 25.0	27.07	S
3	12 22 59.24	18 26 23.3	26.51	S	54	12 22 54.01	18 24 45.7	27.08	S
4	12 22 49.28	18 27 46.1	26.54	S	55	12 22 47.20	18 26 11.2	27.08	S
5	12 22 53.45	18 26 30.0	26.55	S	56	12 22 47.05	18 27 01.0	27.10	S
6	12 22 57.79	18 26 08.0	26.55	S	57	12 22 48.05	18 28 08.0	27.11	S
7	12 22 57.99	18 27 17.2	26.61	S	58	12 22 48.93	18 27 34.1	27.11	S
8	12 22 50.52	18 26 58.6	26.61	S	59	12 22 56.52	18 26 24.7	27.12	S
9	12 22 50.23	18 27 36.2	26.63		60	12 22 55.37	18 24 18.3	27.12	S
10	12 22 55.33	18 27 41.4	26.65		61	12 22 44.52	18 27 57.0	27.16	S
11	12 22 56.48	18 25 48.7	26.67	S	62	12 22 52.48	18 24 34.2	27.16	S
12	12 22 52.29	18 26 48.4	26.69	S	63	12 22 53.97	18 27 00.2	27.17	S
13	12 22 55.55	18 26 54.2	26.70	S	64	12 22 57.83	18 25 40.6	27.18	S
14	12 22 51.31	18 26 12.0	26.70	S	65	12 22 46.51	18 26 12.7	27.22	
15	12 22 54.42	18 26 27.3	26.73	S	66	12 22 56.28	18 25 54.9	27.23	
16	12 22 52.78	18 26 41.8	26.74	S	67	12 22 51.64	18 26 35.0	27.25	
17	12 22 44.55	18 27 14.7	26.75	S	68	12 22 55.03	18 26 11.8	27.26	
18	12 22 47.65	18 27 21.5	26.76	S	69	12 22 45.48	18 25 31.8	27.28	
19	12 22 50.62	18 26 42.6	26.78	S	70	12 22 50.41	18 26 01.9	27.29	
20	12 22 50.33	18 27 25.6	26.78		71	12 22 46.38	18 25 52.0	27.30	
21	12 22 56.66	18 25 31.0	26.79	S	72	12 22 44.99	18 26 52.5	27.31	
22	12 22 56.00	18 27 43.7	26.80	S	73	12 22 58.26	18 28 04.2	27.32	
23	12 22 48.52	18 24 50.7	26.81	S	74	12 22 49.10	18 25 39.4	27.36	
24	12 22 45.36	18 25 57.9	26.85	S	75	12 22 53.80	18 26 19.3	27.36	
25	12 22 45.41	18 24 34.2	26.88	S	76	12 22 57.32	18 26 21.7	27.36	
26	12 22 52.65	18 27 12.1	26.90		77	12 22 46.15	18 28 06.6	27.38	
27	12 22 49.58	18 27 03.7	26.91	S	78	12 22 49.58	18 26 32.3	27.40	
28	12 22 50.87	18 26 38.2	26.92	S	79	12 22 53.54	18 26 25.3	27.44	
29	12 22 54.54	18 27 13.3	26.93	S	80	12 22 46.44	18 26 35.0	27.44	
30	12 22 58.84	18 27 49.4	26.93	S	81	12 22 56.34	18 26 46.1	27.47	
31	12 22 48.98	18 24 42.9	26.93	S	82	12 22 44.95	18 27 02.1	27.49	
32	12 23 00.28	18 26 39.7	26.94	S	83	12 22 57.04	18 25 21.0	27.50	
33	12 22 57.10	18 27 39.0	26.94	S	84	12 22 44.72	18 26 27.6	27.51	
34	12 22 59.93	18 27 59.7	26.96	S	85	12 22 48.83	18 27 47.8	27.53	
35	12 22 53.98	18 25 31.0	26.97	S	86	12 22 51.54	18 26 34.7	27.54	
36	12 22 46.95	18 25 54.3	26.97	S	87	12 22 56.70	18 26 36.5	27.55	
37	12 22 56.10	18 27 16.4	26.98	S	88	12 22 53.64	18 26 37.2	27.55	
38	12 22 57.48	18 27 13.7	26.99	S	89	12 22 47.60	18 26 02.6	27.55	
39	12 22 57.32	18 26 38.2	26.99	S	90	12 22 59.32	18 26 59.1	27.55	
40	12 22 49.26	18 26 20.5	27.00	S	91	12 22 49.62	18 26 36.0	27.58	
41	12 22 49.62	18 24 34.7	27.01	S	92	12 22 46.78	18 27 56.4	27.63	
42	12 22 49.17	18 27 19.7	27.01	S	93	12 22 55.35	18 25 29.9	27.64	
43	12 22 56.61	18 26 43.0	27.01	S	94	12 22 47.26	18 28 08.9	27.66	
44	12 22 55.51	18 25 44.8	27.01	S	95	12 22 52.90	18 25 17.1	27.68	
45	12 22 48.95	18 24 53.8	27.02	S	96	12 22 51.72	18 25 36.4	27.69	
46	12 22 58.35	18 25 30.2	27.02	S	97	12 22 51.14	18 26 26.6	27.79	
47	12 22 58.62	18 25 48.9	27.02	S	98	12 23 00.12	18 25 02.5	27.85	
48	12 22 56.30	18 28 02.3	27.03	S	99	12 22 52.99	18 26 27.7	28.04	
49	12 22 45.56	18 27 46.7	27.04	S	100	12 22 59.21	18 24 39.7	28.12	
50	12 22 54.13	18 24 40.3	27.04	S	101	12 22 57.12	18 24 56.5	28.20	
51	12 22 50.48	18 24 42.7	27.06	S	102	12 22 46.12	18 25 35.7	28.24	

flattening is accurate since the model background is the galaxy itself, faint stars which can contaminate the PN images are completely removed, and the procedure is much less time consuming than analytic flattening methods. However, this process adds noise into the difference image and degrades the signal-to-noise ratio of the PN candidates. For bright objects in nearby galaxies, this added error is not important, but for surveys where the PN are near the limits of the telescope-detector combination and the background noise is considerable, the problem cannot be tolerated. Two different procedures were therefore used to flatten the galaxy background and improve the photometric measurements.

For those fields taken at Kitt Peak, the readout noise of the TI2 CCD was low enough so that the PN could be measured on the difference image without degrading the quality of the photometry. However, while the dominant noise source in the Kitt Peak data was background galaxy light, measurements on the CFHT images were limited by readout noise. Therefore, although we did perform a differencing operation on the CFHT frames to reveal any large-scale emission and star-formation zones (which needed to be avoided when identifying PN candidates), we did not perform actual measurements on these data. Instead, we fitted a two-dimensional planar surface to the small region (64 pixels square) immediately surrounding

TABLE 6
 NGC 4406 PLANETARY NEBULAE

ID	$\alpha(1950)$	$\delta(1950)$	m_{5007}	Sample	ID	$\alpha(1950)$	$\delta(1950)$	m_{5007}	Sample
1	12 23 41.28	13 14 17.1	25.61		72	12 23 27.40	13 14 52.9	27.19	S
2	12 23 29.92	13 12 03.4	26.30		73	12 23 45.26	13 13 03.6	27.20	S
3	12 23 39.38	13 14 07.3	26.32		74	12 23 33.98	13 14 38.0	27.21	
4	12 23 43.04	13 13 31.1	26.56		75	12 23 25.52	13 13 27.4	27.21	
5	12 23 37.06	13 13 52.6	26.57		76	12 23 46.23	13 11 26.1	27.22	
6	12 23 39.92	13 14 21.2	26.57		77	12 23 54.35	13 12 07.3	27.23	
7	12 23 48.24	13 13 19.4	26.57	S	78	12 23 32.08	13 12 07.1	27.23	
8	12 23 39.22	13 14 31.4	26.58	S	79	12 23 32.40	13 15 10.9	27.24	
9	12 23 55.68	13 11 58.8	26.58	S	80	12 23 46.97	13 11 18.7	27.24	
10	12 23 45.20	13 12 20.9	26.63	S	81	12 23 33.58	13 12 44.2	27.24	
11	12 23 25.53	13 12 10.5	26.65	S	82	12 23 46.16	13 11 07.1	27.25	
12	12 23 38.80	13 15 07.6	26.69	S	83	12 23 36.04	13 14 30.8	27.28	
13	12 23 38.60	13 14 22.0	26.73		84	12 23 33.64	13 15 39.7	27.29	
14	12 23 48.33	13 12 20.4	26.73	S	85	12 23 49.65	13 12 43.2	27.29	
15	12 23 52.48	13 11 45.8	26.73	S	86	12 23 46.87	13 12 40.0	27.31	
16	12 23 38.54	13 12 23.7	26.75	S	87	12 23 49.90	13 13 43.3	27.31	
17	12 23 37.58	13 13 56.9	26.77		88	12 23 51.51	13 12 15.9	27.33	
18	12 23 40.62	13 14 24.9	26.79	S	89	12 23 46.98	13 12 25.8	27.33	
19	12 23 54.56	13 12 50.0	26.79	S	90	12 23 35.87	13 14 40.8	27.33	
20	12 23 46.66	13 13 29.6	26.80	S	91	12 23 45.40	13 14 20.2	27.34	
21	12 23 36.48	13 14 12.8	26.80		92	12 23 51.53	13 13 26.4	27.34	
22	12 23 51.51	13 12 08.5	26.82	S	93	12 23 28.65	13 14 09.6	27.35	
23	12 23 40.53	13 10 47.7	26.83	S	94	12 23 44.68	13 12 09.0	27.37	
24	12 23 35.63	13 14 04.4	26.85		95	12 23 36.82	13 14 14.9	27.39	
25	12 23 38.42	13 12 15.2	26.85	S	96	12 23 37.28	13 14 22.8	27.41	
26	12 23 53.56	13 11 24.1	26.85	S	97	12 23 30.78	13 13 00.7	27.41	
27	12 23 33.51	13 12 04.1	26.86	S	98	12 23 33.08	13 13 31.5	27.42	
28	12 23 34.67	13 13 43.3	26.87		99	12 23 45.86	13 12 34.4	27.43	
29	12 23 52.88	13 13 16.9	26.87	S	100	12 23 48.57	13 11 58.3	27.45	
30	12 23 28.39	13 12 57.2	26.88	S	101	12 23 46.45	13 12 34.6	27.46	
31	12 23 32.78	13 12 26.1	26.88	S	102	12 23 32.71	13 14 17.5	27.47	
32	12 23 37.36	13 12 53.7	26.88		103	12 23 26.22	13 14 23.8	27.48	
33	12 23 31.86	13 15 15.5	26.88	S	104	12 23 51.77	13 12 45.8	27.48	
34	12 23 28.43	13 15 34.6	26.89	S	105	12 23 33.31	13 14 42.7	27.49	
35	12 23 35.87	13 14 39.0	26.90	S	106	12 23 46.03	13 10 55.5	27.49	
36	12 23 32.39	13 13 40.8	26.90	S	107	12 23 51.84	13 13 20.8	27.52	
37	12 23 27.36	13 13 41.0	26.91	S	108	12 23 41.48	13 11 52.3	27.53	
38	12 23 31.96	13 14 06.4	26.91	S	109	12 23 48.10	13 11 49.7	27.53	
39	12 23 35.77	13 12 21.7	26.92	S	110	12 23 53.84	13 12 07.3	27.55	
40	12 23 45.08	13 14 37.0	26.92	S	111	12 23 49.88	13 12 57.0	27.55	
41	12 23 37.90	13 12 09.0	26.94	S	112	12 23 44.06	13 12 01.3	27.56	
42	12 23 36.47	13 12 42.1	26.94	S	113	12 23 25.13	13 14 17.7	27.59	
43	12 23 47.60	13 12 21.8	26.94	S	114	12 23 33.20	13 14 25.2	27.59	
44	12 23 37.57	13 12 52.0	26.95		115	12 23 35.18	13 13 52.7	27.60	
45	12 23 37.71	13 13 13.1	26.95		116	12 23 52.46	13 11 40.8	27.64	
46	12 23 30.62	13 14 21.8	26.95	S	117	12 23 49.04	13 12 34.7	27.64	
47	12 23 45.05	13 13 39.1	26.96	S	118	12 23 47.18	13 11 18.0	27.65	
48	12 23 36.18	13 15 40.1	26.96	S	119	12 23 46.37	13 11 21.0	27.67	
49	12 23 49.39	13 12 23.3	26.97	S	120	12 23 53.17	13 10 53.1	27.68	
50	12 23 53.34	13 10 55.7	26.99	S	121	12 23 47.43	13 12 12.6	27.73	
51	12 23 46.58	13 11 39.5	27.00	S	122	12 23 29.70	13 13 41.3	27.73	
52	12 23 32.18	13 12 37.3	27.01	S	123	12 23 47.12	13 10 58.3	27.73	
53	12 23 31.24	13 13 51.5	27.03	S	124	12 23 36.98	13 14 04.4	27.76	
54	12 23 53.81	13 12 14.6	27.04	S	125	12 23 48.25	13 12 11.7	27.80	
55	12 23 39.53	13 15 19.0	27.05	S	126	12 23 28.64	13 12 49.5	27.81	
56	12 23 49.95	13 13 29.4	27.05	S	127	12 23 47.42	13 10 49.2	27.84	
57	12 23 48.79	13 13 06.6	27.08	S	128	12 23 44.57	13 11 51.6	27.86	
58	12 23 31.32	13 13 37.7	27.08	S	129	12 23 37.11	13 14 20.8	27.89	
59	12 23 51.09	13 12 11.5	27.08	S	130	12 23 25.20	13 13 27.2	27.89	
60	12 23 32.58	13 12 13.5	27.09	S	131	12 23 51.31	13 10 51.6	27.92	
61	12 23 47.77	13 12 38.9	27.10	S	132	12 23 44.18	13 11 33.4	27.94	
62	12 23 28.76	13 15 27.2	27.10	S	133	12 23 33.25	13 14 26.5	27.95	
63	12 23 27.89	13 15 41.1	27.10	S	134	12 23 32.38	13 12 34.7	27.98	
64	12 23 35.00	13 14 28.7	27.11	S	135	12 23 46.52	13 12 32.2	28.00	
65	12 23 32.19	13 14 49.6	27.12	S	136	12 23 24.88	13 12 58.1	28.01	
66	12 23 32.95	13 13 14.9	27.12	S	137	12 23 46.69	13 12 34.6	28.05	
67	12 23 35.64	13 12 26.0	27.15	S	138	12 23 48.32	13 11 39.3	28.11	
68	12 23 41.17	13 10 48.8	27.16	S	139	12 23 46.55	13 10 54.9	28.12	
69	12 23 26.67	13 13 16.7	27.18	S	140	12 23 48.87	13 11 54.5	28.28	
70	12 23 43.90	13 12 24.3	27.18	S	141	12 23 37.33	13 14 25.1	28.31	
71	12 23 30.37	13 14 06.0	27.18	S					

TABLE 7
NGC 4472 PLANETARY NEBULAE

ID	$\alpha(1950)$	$\delta(1950)$	m_{5007}	Sample	ID	$\alpha(1950)$	$\delta(1950)$	m_{5007}	Sample
1	12 27 17.48	8 16 54.7	26.19		28	12 27 10.03	8 17 24.0	26.91	S
2	12 27 18.78	8 18 13.8	26.26	S	29	12 27 18.11	8 18 03.0	26.91	S
3	12 27 19.85	8 15 03.1	26.37	S	30	12 27 08.41	8 17 49.7	26.93	S
4	12 27 20.90	8 15 48.3	26.40	S	31	12 27 18.53	8 15 56.1	26.95	S
5	12 27 11.27	8 16 03.2	26.46		32	12 27 15.22	8 17 29.2	26.97	S
6	12 27 19.27	8 16 59.5	26.48	S	33	12 27 13.01	8 18 25.4	26.98	S
7	12 27 18.25	8 18 15.4	26.56	S	34	12 27 06.91	8 18 48.0	26.99	S
8	12 27 11.88	8 15 14.0	26.61	S	35	12 27 12.37	8 14 20.2	27.00	S
9	12 27 13.96	8 17 23.6	26.61		36	12 27 10.90	8 18 30.3	27.07	
10	12 27 19.38	8 15 52.9	26.64	S	37	12 27 15.90	8 17 12.6	27.08	
11	12 27 15.66	8 15 15.5	26.64	S	38	12 27 10.90	8 18 30.3	27.09	
12	12 27 14.24	8 17 57.1	26.64	S	39	12 27 16.12	8 15 09.9	27.13	
13	12 27 08.94	8 17 17.6	26.72	S	40	12 27 09.85	8 18 17.7	27.17	
14	12 27 13.02	8 15 20.6	26.73	S	41	12 27 17.78	8 18 23.3	27.26	
15	12 27 17.64	8 17 50.9	26.74	S	42	12 27 13.24	8 17 21.0	27.27	
16	12 27 18.06	8 15 12.6	26.74	S	43	12 27 09.18	8 18 18.7	27.30	
17	12 27 11.04	8 15 16.3	26.77	S	44	12 27 09.72	8 16 53.6	27.30	
18	12 27 11.81	8 17 09.6	26.81		45	12 27 09.37	8 17 44.0	27.41	
19	12 27 16.43	8 14 19.1	26.81	S	46	12 27 21.77	8 16 10.3	27.44	
20	12 27 13.34	8 17 23.8	26.81		47	12 27 19.68	8 15 31.4	27.47	
21	12 27 13.42	8 14 11.1	26.81	S	48	12 27 09.94	8 18 37.6	27.47	
22	12 27 17.23	8 17 27.9	26.82	S	49	12 27 06.65	8 18 28.6	27.50	
23	12 27 14.66	8 15 43.7	26.84		50	12 27 16.02	8 15 09.7	27.53	
24	12 27 14.51	8 17 40.8	26.85		51	12 27 08.36	8 18 12.6	27.59	
25	12 27 21.72	8 15 14.6	26.90	S	52	12 27 08.94	8 18 17.6	27.61	
26	12 27 16.91	8 14 31.7	26.90	S	53	12 27 19.38	8 15 17.9	27.73	
27	12 27 09.06	8 17 58.8	26.91	S	54	12 27 10.22	8 15 53.3	27.80	

TABLE 8
NGC 4486 PLANETARY NEBULAE

ID	$\alpha(1950)$	$\delta(1950)$	m_{5007}	Sample	ID	$\alpha(1950)$	$\delta(1950)$	m_{5007}	Sample
1	12 28 17.53	12 37 31.9	25.57		29	12 28 11.17	12 41 03.1	27.01	S
2	12 28 20.61	12 37 47.1	26.01		30	12 28 17.19	12 38 35.8	27.02	S
3	12 28 13.63	12 38 35.0	26.03		31	12 28 15.93	12 41 16.6	27.06	S
4	12 28 14.22	12 36 11.7	26.21		32	12 28 18.92	12 37 50.0	27.09	S
5	12 28 12.02	12 37 12.9	26.44	S	33	12 28 16.36	12 38 18.1	27.10	S
6	12 28 17.84	12 38 37.7	26.45	S	34	12 28 18.42	12 37 35.6	27.11	S
7	12 28 19.72	12 36 14.5	26.50	S	35	12 28 24.41	12 37 41.3	27.12	S
8	12 28 15.72	12 37 59.2	26.60	S	36	12 28 23.36	12 38 04.5	27.13	S
9	12 28 21.05	12 41 43.7	26.70	S	37	12 28 14.82	12 41 03.9	27.15	S
10	12 28 16.12	12 37 45.8	26.71	S	38	12 28 20.48	12 37 05.7	27.16	S
11	12 28 18.62	12 36 39.9	26.74	S	39	12 28 14.70	12 38 30.1	27.16	S
12	12 28 15.15	12 41 52.5	26.75	S	40	12 28 23.20	12 40 18.1	27.19	S
13	12 28 18.38	12 41 42.7	26.76	S	41	12 28 22.87	12 38 47.5	27.20	S
14	12 28 15.22	12 41 38.9	26.76	S	42	12 28 19.03	12 41 19.2	27.25	
15	12 28 24.72	12 40 48.1	26.77	S	43	12 28 18.16	12 37 42.8	27.28	
16	12 28 22.92	12 37 25.5	26.81	S	44	12 28 10.98	12 40 24.6	27.31	
17	12 28 15.10	12 41 09.3	26.82	S	45	12 28 24.41	12 40 52.4	27.34	
18	12 28 21.38	12 40 27.5	26.84		46	12 28 13.38	12 41 32.0	27.44	
19	12 28 22.46	12 36 35.2	26.84	S	47	12 28 20.52	12 36 41.6	27.67	
20	12 28 12.58	12 40 21.5	26.87	S	48	12 28 12.42	12 41 32.9	27.79	
21	12 28 19.63	12 36 27.3	26.89	S	49	12 28 09.75	12 38 30.3	27.81	
22	12 28 24.57	12 37 59.4	26.91	S	50	12 28 22.90	12 40 37.0	27.93	
23	12 28 22.67	12 38 48.0	26.92	S	51	12 28 22.81	12 35 37.5	28.01	
24	12 28 12.00	12 37 57.3	26.97	S	52	12 28 24.37	12 37 45.0	28.03	
25	12 28 14.99	12 37 16.8	26.99	S	53	12 28 14.48	12 37 12.5	28.05	
26	12 28 21.43	12 37 52.3	27.00	S	54	12 28 23.17	12 37 25.1	28.11	
27	12 28 22.88	12 40 39.7	27.00	S	55	12 28 18.66	12 41 12.3	28.15	
28	12 28 24.57	12 35 39.4	27.00	S					

TABLE 9
NGC 4649 PLANETARY NEBULAE

ID	$\alpha(1950)$	$\delta(1950)$	m_{5007}	Sample
1	12 41 10.69	11 48 13.5	26.40	S
2	12 41 04.66	11 49 13.5	26.45	S
3	12 41 10.10	11 49 12.6	26.49	S
4	12 41 09.57	11 48 24.8	26.51	S
5	12 41 02.26	11 49 18.3	26.61	S
6	12 41 12.58	11 49 17.1	26.62	S
7	12 41 04.62	11 49 23.4	26.62	S
8	12 41 10.86	11 49 11.8	26.65	S
9	12 41 08.72	11 49 04.2	26.68	S
10	12 41 11.16	11 48 50.8	26.68	S
11	12 41 03.32	11 48 27.8	26.80	S
12	12 41 08.30	11 48 54.4	26.82	S
13	12 41 10.32	11 46 47.2	26.82	S
14	12 41 08.03	11 48 32.5	26.84	S
15	12 41 08.69	11 49 00.4	26.88	S
16	12 41 05.92	11 48 53.4	26.88	S
17	12 41 15.98	11 46 40.7	26.90	S
18	12 41 07.95	11 48 41.7	26.95	
19	12 41 16.30	11 47 13.0	27.01	
20	12 41 05.98	11 48 10.1	27.06	
21	12 41 05.59	11 48 05.8	27.08	
22	12 41 01.52	11 46 14.6	27.10	
23	12 41 14.99	11 49 21.0	27.15	
24	12 41 12.30	11 49 10.1	27.17	
25	12 41 15.69	11 46 47.9	27.28	
26	12 41 15.34	11 49 27.2	27.46	
27	12 41 02.20	11 49 24.7	27.52	
28	12 41 01.13	11 49 17.9	27.52	
29	12 41 08.46	11 46 42.1	27.54	
30	12 41 01.45	11 49 16.7	27.58	
31	12 41 08.33	11 47 19.4	27.86	
32	12 41 07.90	11 46 08.2	28.10	

each PN candidate and subtracted this model surface from the original image. This simple procedure flattened the underlying background in the immediate vicinity of each object to a high degree of precision. (In principle, we could have flattened the entire field by modeling the overall galaxy surface brightness, but the local approach is simpler and less susceptible to field anomalies such as companion galaxies and dust lanes.)

Once the region around each PN was flattened, we proceeded with the photometric measurements. First three to five well isolated field stars were chosen to define the frame point-spread function (PSF). Ideally, these stars were located far away from the galactic nucleus where the gradient in the background luminosity was small. Unfortunately, this was not always possible, so, in those cases where a PSF star was projected on a region with a strong luminosity gradient, the analytic sky flattening algorithm was again used to remove the varying background. (The difference technique, of course, cannot be used on stars, since they are continuum objects.) The PSF photometry package of DAOPHOT (Stetson 1987) was then used to measure both the PN and a set of comparison stars.

To place these instrumental magnitudes on the standard system, we performed simulated aperture photometry on several field stars using apertures ~ 6 times the FWHM of the seeing disk. We then converted these magnitudes to apparent flux by comparing these measurements with measurements obtained on Stone (1977) and Oke (1974) spectrophotometric standards, modeling the filter transmission curve for the effects of telescope f /ratio, ambient temperature, and stellar velocity

TABLE 10
VIRGO ASTROMETRIC REFERENCE STARS

Galaxy	ID	$\alpha(1950)$	$\delta(1950)$
NGC 4374	a	12 22 23.24	13 11 37.1
	b	12 22 23.95	13 11 25.9
	c	12 22 25.85	13 09 32.3
	d	12 22 26.94	13 09 17.3
	e	12 22 37.45	13 09 56.4
	f	12 22 43.12	13 09 14.4
	g	12 22 42.63	13 08 45.6
	h	12 22 39.77	13 08 30.5
NGC 4382	a	12 22 55.74	18 27 12.8
	b	12 22 52.73	18 27 19.2
	c	12 22 48.15	18 27 30.1
	d	12 22 44.30	18 25 45.9
	e	12 22 55.66	18 24 24.6
	f	12 22 51.45	18 27 30.0
NGC 4406	a	12 23 52.73	13 14 16.1
	b	12 23 52.46	13 13 35.9
	c	12 23 48.34	13 12 38.0
	d	12 23 41.80	13 14 33.7
	e	12 23 31.33	13 15 02.0
	f	12 23 28.93	13 15 19.0
	g	12 23 37.29	13 13 34.0
	h	12 23 38.57	13 12 58.8
NGC 4472	a	12 27 09.42	8 17 20.4
	b	12 27 07.94	8 17 32.2
	c	12 27 12.47	8 17 41.6
	d	12 27 14.50	8 18 09.3
	e	12 27 13.96	8 14 21.1
	f	12 27 13.24	8 14 37.9
	g	12 27 09.06	8 15 30.4
NGC 4486	a	12 28 15.55	12 38 21.7
	b	12 28 10.14	12 35 40.7
	c	12 28 23.14	12 37 14.1
	d	12 28 11.57	12 41 50.5
	e	12 28 15.90	12 41 03.8
	f	12 28 20.96	12 40 56.1
NGC 4649	a	12 41 03.07	11 48 41.3
	b	12 41 10.49	11 47 27.6
	c	12 41 10.02	11 47 12.7
	d	12 41 08.76	11 45 56.3
	e	12 41 02.19	11 45 58.0

dispersion (Table 11) as described in Paper III, and using the photometric procedures for emission-line objects described by Jacoby, Quigley, and Africano (1987). Corrections for atmospheric extinction were calculated assuming standard extinction models for CFHT ($A_{5007} = 0.16$ mag-airmass $^{-1}$) and KPNO ($A_{5007} = 0.17$ mag-airmass $^{-1}$). The apparent magnitudes for the PN candidates in each galaxy, transformed to m_{5007} following the relation defined in Paper I ($m_{5007} = -2.5 \log F_{5007} - 13.74$), are presented in Tables 4–9.

For each galaxy with more than one survey field, we obtained an extra frame centered on the galaxy's nucleus, in order to improve the photometry and astrometry by tying the two fields together through measurements in the regions of field overlap (cf. Ciardullo *et al.* 1987). Initially, it appeared that there would be an adequate number of isolated objects to perform this function. Unfortunately, when examined carefully, most of these potential tie-in stars were found to be marginally extended, indicating that they are either bright globular clus-

TABLE 11
SUMMARY FOR VIRGO GALAXIES

Parameter	NGC 4374	NGC 4382	NGC 4406	NGC 4472	NGC 4486	NGC 4649
PN magnitude completeness limit	27.3	27.2	27.2	27.0	27.2	26.9
Inner isophotal radius for sample	105"	60"	80"	80"	75"	30"
Inner isophote V surface brightness	22.51 ^a	20.95: ^b	21.52 ^c	21.06 ^c	21.31 ^c	19.85 ^d
V_{sampled}	11.16 ^a	10.67: ^b	10.19 ^c	10.24 ^c	10.48 ^c	10.35 ^d
Adopted bolometric correction	-0.83	-0.67	-0.79	-0.85	-0.85	-0.85
Total number of PN found	102	102	141	54	55	32
Number of PN in complete sample	37	59	59	26	36	16
Adopted velocity dispersion (km s ⁻¹)	230 ^e	200 ^f	200 ^e	230 ^e	260 ^g	250 ^h
Most likely distance modulus	30.98	30.79	30.98	30.71	30.81	30.76
Most likely distance (Mpc)	15.7 ± 0.5	14.4 ± 0.4	15.7 ± 0.4	13.9 ± 0.6	14.5 ± 0.4	14.2 ± 0.6
Most likely specific PN density ($\alpha_{2.5} \times 10^9$)	16.7 ± 3.1	19.7 ± 2.8:	13.3 ± 2.0	6.5 ± 1.4	8.3 ± 1.5	6.4 ± 2.0
Implied stellar death rate ($\times 10^{12}$)	6.8	8.0:	5.4	2.7	3.4	2.6

^a From the calibration of the combined surface photometry of Lauer 1985, Jedrzejewski 1987, and Michard 1985.

^b Approximation based on the calibration of surface photometry by Michard 1985.

^c From the calibration of surface photometry by Cohen 1986.

^d From the calibration of the combined surface photometry of Lauer 1985, Djorgovski 1985, and Michard 1985.

^e Estimated from the velocity dispersion profile of Davies 1981.

^f Taken from Whitmore, McElroy, and Tonry 1985.

^g Estimated from the velocity dispersion profile of Sargent *et al.* 1978.

^h Estimated from the velocity dispersion profile of Franx, Illingworth, and Heckman 1989.

ters or companion dwarf galaxies, and therefore unsuitable for accurate photometry. (Although it is possible, in principle, to use the underlying galaxy to tie fields together, the uncertainties involved in performing surface photometry on galaxies much larger than the CCD field outweigh the potential gains.) As a result, we were able to use the KPNO photometric tie-in frames only for NGC 4472 and 4486, while the two fields of NGC 4374 and 4406 had to be calibrated independently. (The remaining two galaxies, NGC 4382 and 4649, were surveyed in only one field.) Fortunately, every usable night for this project was photometric; hence the errors in the photometric zero points are small.

(A curious situation arose when we evaluated the quality of the photometry in the two fields of NGC 4472: the residuals of the photometric transfer stars in the tie-in frames were much higher than expected. We eventually traced the problem to the stars in the northern field, and discovered that one of them [NGC 4472b in Table 10] had varied between the time of the CFHT survey and the tie-in observation. Subsequent observations of this star demonstrated that the object is a distant RR Lyrae star in the halo of our Galaxy with $\langle V \rangle = 19.23$ [Ciardullo, Jacoby, and Bond 1989]).

IV. DERIVING THE DISTANCES

We derived distances to the galaxies by fitting the observed PNLf to an empirical model using the methods described in Papers II, III, and IV. The process requires (1) a proper statistical sample of PN that is unaffected by observational selection effects, (2) an estimate for the distribution of photometric errors as a function of magnitude, and (3) an estimate for foreground extinction.

a) Defining the Statistically Complete Samples

As in Paper IV, we histogrammed the PN magnitudes in each galaxy to produce six raw luminosity functions (Fig. 2). As we look to fainter magnitudes, the number of PN candidates increases sharply, beginning in each case near an [O III] magnitude $m_{5007} \sim 26.4$, again confirming the utility of these objects as standard candles. The PNLfs then rise for about 1 mag, until incompleteness becomes important at $m_{5007} \sim 27.2$. Note

that the PNLfs for NGC 4374, 4382, 4406, and 4486 include several objects that are distinctly brighter than the PNLf cutoff at $m_{5007} \sim 26.4$. This is a new phenomenon: no such overluminous emission-line objects were detected in our previous surveys. For consistency, we therefore discarded these objects from the analysis; if we forced the model PNLf to include these points we would derive significantly smaller distances and have much poorer fits. We will discuss these objects further in § Vv.

The data displayed in Figure 2 are not statistically complete, as evidenced by the decreasing number of identifications at the faint end. In addition, some bright PN probably have been missed near the galaxy centers where the galaxy background is high. Therefore, we cannot compare these PNLfs with those in other galaxies without taking these selection effects into account, and defining proper statistical PN samples.

As explained in Papers II, III, and IV, the best way to determine the incompleteness in a sample of planetaries is to examine the luminosity specific number density of PN as a function of position in the galaxy. Theoretical calculations predict that this quantity, α , should be insensitive to the age or initial mass function of a stellar population (Renzini and Buzzoni 1986). Observations in M31, M81, and the Leo Group galaxies support this claim: to date, no significant radial gradient in α has been seen. Consequently, by comparing the luminosity specific PN number density with background surface brightness, regions of incompleteness in the PN samples can be found.

In order to perform this comparison, the luminosity distribution of each galaxy was modeled with a series of concentric elliptical isophotes with varying axial ratios and position angles. Because our observations extended farther into the halo than most other CCD surveys, this required combining a number of different studies. For NGC 4406, NGC 4472, and NGC 4486, our models used the CCD surface photometry of Cohen (1986), which included data taken over $5'$ away from the nucleus. The models of NGC 4374 and NGC 4649, however, required merging the inner region CCD photometry of Lauer (1985), Jedrzejewski (1987), and Djorgovski (1985) with the halo photographic photometry of Michard (1985). NGC 4382

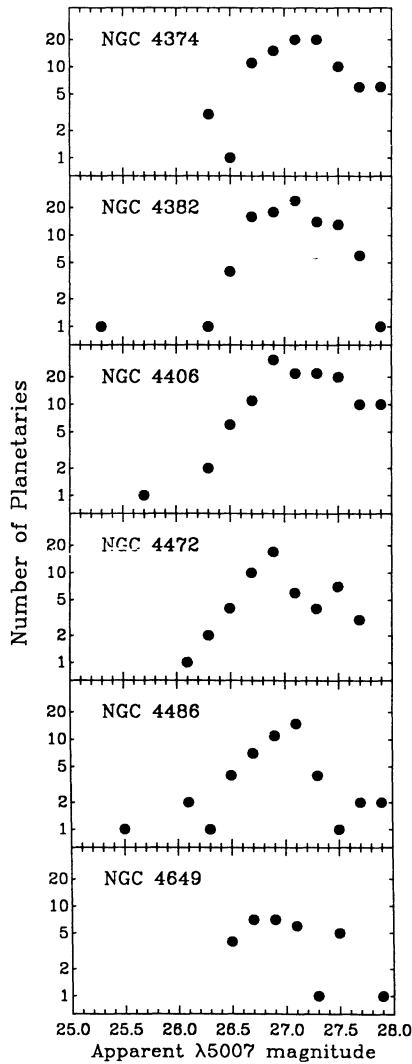


FIG. 2.—The raw planetary nebula luminosity functions for the six Virgo galaxies binned into intervals of 0.2 mag. Magnitudes are defined as in Paper I, where $m_{5007} = -2.5 \log F_{5007} - 13.74$. Although these samples are heterogeneous in that they contain PN below the completeness limit and at small galaxy radii, the similarity in shape and bright end cutoff luminosity is evident. Note the overluminous objects in NGC 4382, NGC 4406, and NGC 4486. These are discussed in § Vc. The observations of NGC 4649 were limited by poor seeing, hence the small number of planetaries.

was modeled entirely with the photographic photometry of Michard, although, since this galaxy is undergoing an interaction and has irregular isophotes, this model probably is not very accurate.

After adopting these models, the isophotal radial distance of each planetary from the center of its parent galaxy was calculated by finding the semimajor axis of the isophote upon which it was superposed. The distribution of these distances was then compared to the distribution of light along the galaxy's major axis, corrected for the fraction of luminosity enclosed in the survey regions. Figure 3 performs this comparison for PN at the nominal completeness limit of each galaxy (cf. Table 11). For most of the galaxies, the agreement at large radii is excellent: except for NGC 4382, the disturbed galaxy with poorly modeled isophotes, and NGC 4649, a galaxy whose PN observations were limited by 1.6" seeing, the PN follow the halo light

exceedingly well. However, in all cases, the luminosity specific PN density in the inner envelope falls precipitously at small radii, indicating that incompleteness is important in regions of high surface brightness. We therefore excluded these areas from our analysis. Table 11 summarizes the completeness limits for each galaxy; those PN which are members of the statistical samples are indicated in Tables 4–9 with an "S."

b) Estimating the Photometric Errors

To properly compare our empirical PNLf to observations, this empirical curve must be convolved with a function which reproduces the photometric error. Thus the variation of observational error versus magnitude for the statistical sample of PN is needed. To estimate this, the theoretical measurement error of each PN was found using DAOPHOT (Stetson 1987). We then binned the PN into 0.2 mag intervals and computed

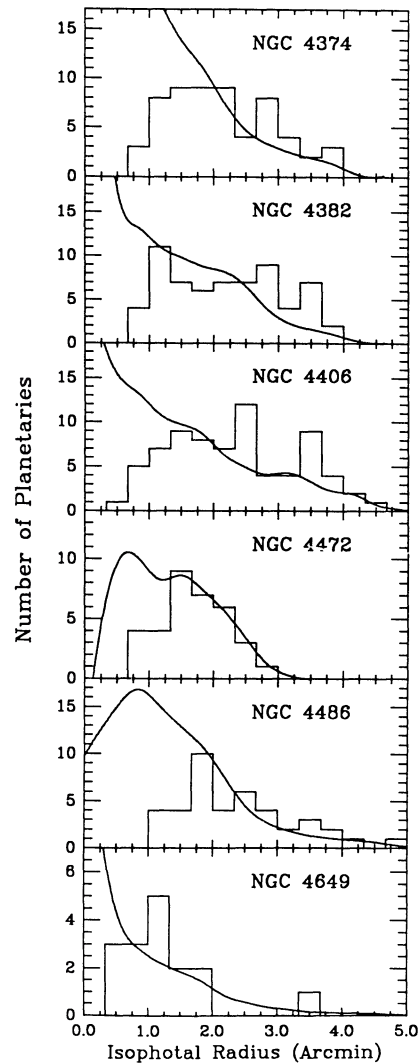


FIG. 3.—Histograms showing the distribution of isophotal radii for PN candidates brighter than the completeness limit. The solid lines display the amount of luminosity surveyed in each galaxy. A comparison of these curves with the data shows that in the inner regions of the galaxies, incompleteness is important, as PN are being lost amid the bright background. In the outer areas, however, no significant gradient in the luminosity specific PN density is seen. The curve for NGC 4382 is only approximate, as the galaxy has irregular isophotes.

TABLE 12
PLANETARY NEBULAE PHOTOMETRIC ERROR (σ) vs. MAGNITUDE FOR VIRGO GALAXIES

Magnitude	NGC 4374	NGC 4382	NGC 4406	NGC 4472	NGC 4486	NGC 4649
26.2.....	0.069	0.033	0.064	0.091	0.042	...
26.4.....	0.073	0.107	0.060	0.091
26.6.....	0.089	0.080	0.098	0.133	0.071	0.115
26.8.....	0.105	0.100	0.109	0.149	0.090	0.129
27.0.....	0.125	0.117	0.128	0.179	0.116	0.144
27.2.....	0.148	0.134	0.164	0.209	0.139	0.161
27.4.....	0.170	0.153	0.192	0.245	0.164	0.192

the mean error for the objects in each bin. These errors are underestimates of the true photometric error since they are based only on theoretical detector performance and exclude uncertainties due to flat-fielding, local sky flattening, and low-level radiation events. The estimates are still useful, however, as our results are insensitive to the precise value of the errors: a 30% increase in the photometric uncertainty extends the distance to Virgo by less than 2%. The smoothed distribution of photometric error versus magnitude for each galaxy is listed in Table 12. When no PN were found in a bin, the error could not be computed, and so we interpolated across those bins during the convolution with the model PNLF.

c) Estimate of the Foreground Extinction

In contrast to the long-standing disagreement over the distance to Virgo, estimates for the foreground interstellar extinction toward these galaxies are remarkably consistent. For example, the global formulae of Sandage (1973), Burstein and McDonald (1975), and de Vaucouleurs, de Vaucouleurs, and Corwin (1976; RC2) yield reddening values toward NGC 4486 of $E(B-V) = 0.0, 0.023,$ and $0.049,$ respectively, while the Burstein and Heiles (1982) reddening maps show no evidence of extinction in the cluster's direction. Perhaps the best measurement of the extinction toward Virgo is the 21 cm H I observations by Burstein and Heiles (1984), which give a mean differential extinction toward our six Virgo galaxies of $E(B-V) = 0.017 \pm 0.014.$ (Unless otherwise noted, all quoted errors refer to unweighted 1σ standard deviations.)

While we could simply adopt the individual extinction measurements given by Burstein and Heiles (1984) for the six galaxies, the quoted uncertainty in each value, 0.015 mag in $E(B-V),$ is a significant fraction of the estimated reddenings. In fact, the reddening is negative to NGC 4472, an artifact of the noise in the measurements. Instead, we assume that the foreground extinction is identical to each galaxy and that the Burstein and Heiles (1984) values represent six independent measurements of this quantity. When combined with Seaton's (1979) expression for extinction as a function of wavelength, the differential reddening of $E(B-V) = 0.017 \pm 0.006$ (error of the mean) corresponds to a total extinction at $\lambda 5007$ of 0.061 mag.

d) Fitting the PNLFs

As demonstrated in M81 (Paper III) and the Leo Group galaxies NGC 3377, 3379, and 3384 (Paper IV), the empirical PNLF defined by observations of PN in M31 (Paper II) is an excellent representation of the true luminosity function. We therefore derived distances for the six Virgo galaxies by fitting the observed PNLF with the empirical law using the maximum likelihood techniques described in Paper II. A by-product of this procedure, however, is an estimate of the total size of a

galaxy's PN population, which, when normalized to the amount of luminosity surveyed, gives the luminosity specific stellar death rate. Since the theory of stellar energy generation says that this death rate is insensitive to the age or initial mass function of a stellar population (Renzini and Buzzoni 1986), this number provides a check on the results of the maximum likelihood calculation. An estimate of the total bolometric luminosity enclosed within each of our survey fields is therefore required.

To calculate this quantity, the heterogeneous combination of surface photometry described in § IVa was transformed into a homogeneous set of V -band luminosity profiles using B and V galaxy photometry performed with the TEK1 CCD at the f/7.5 focus of the Kitt Peak No. 1 0.9 m telescope on 1989 April 9 and 11. Surface photometry of the inner regions of each galaxy was carried out with the GASP photometry package (Cawson 1983) and the resulting luminosity profiles were compared to the previously adopted profiles derived from the literature. Magnitude offsets were then applied to the model galaxies to place each profile on the standard V system. The total V magnitude surveyed within each galaxy was then calculated by integrating the models over the PN survey regions. Since the scatter in the reduced magnitudes of the ~ 20 Landolt (1973, 1983) standard stars observed each night was less than 0.02 mag, the error introduced by our zero point offsets is insignificant compared to the uncertainties in the adopted luminosity distributions.

After computing these V magnitudes, an effective bolometric correction for each galaxy was calculated. This was done by combining the optical colors of Poulain (1988) and Michard (1982) with the infrared colors of Frogel *et al.* (1978) and comparing the derived bolometric fluxes to those found for a library of stellar spectra (cf. Paper II). These corrections were then added to the enclosed V magnitudes to yield the total bolometric magnitude surveyed within each galaxy.

The maximum likelihood solutions and the formal errors for the six Virgo galaxies included in our survey are presented in Table 11. Figure 4 illustrates the goodness of the fits by overplotting the statistically complete PNLFs and the best-fit empirical PNLF convolved with the photometric error function from Table 12. Figure 5 illustrates the uncertainty in the results by plotting the probability of the solution as a function of distance modulus and luminosity specific PN density. From Table 11, the mean distance to the six galaxies is 14.7 ± 0.8 Mpc. If we had adopted a value for the foreground extinction of exactly 0.0, all distances would increase by ~ 0.4 Mpc, and the average distance would be 15.1 Mpc. Note that NGC 4406 is clearly a member of the Virgo Cluster and not a foreground galaxy, despite its negative velocity.

We checked that the derived distances are internally consistent in the following manner. First we shifted the magnitudes

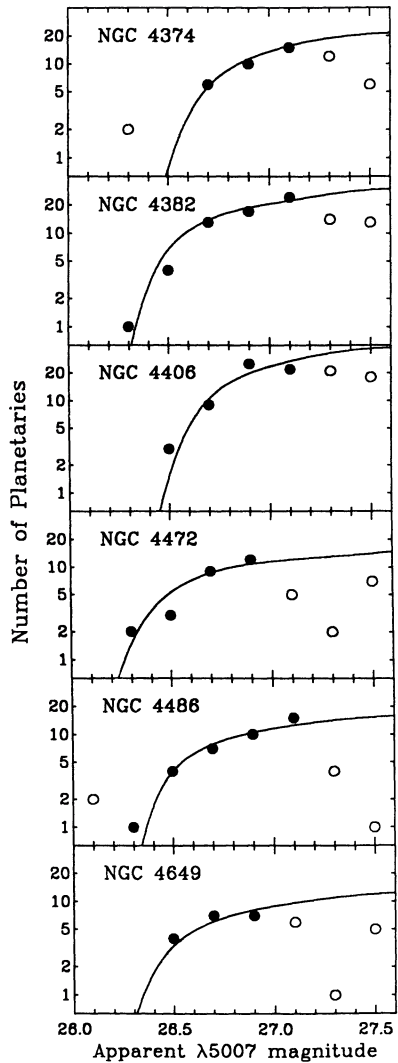


FIG. 4.—The planetary nebula luminosity functions for the six Virgo galaxies based on the homogeneous and complete samples. The data are binned into 0.2 mag intervals. The solid lines show the empirical PNLF convolved with the mean photometric error vs. magnitude relations and translated to the most likely apparent distance moduli. Open circles represent overluminous objects or PN below the completeness limit and have not been included in the fits.

of the observed PNLF of each galaxy to our mean distance to the cluster. We then combined the PNLFs (excluding those objects outside our regions of completeness) into a single grand luminosity function. This function is displayed in Figure 6. Note that, although there is clearly a small population of overluminous objects which contaminates the sample, the model fits the distribution of PN magnitudes exceptionally well and gives an unambiguous result. Using the maximum likelihood procedures of Paper II, we get a distance to the statistical sample of PN of 14.9 ± 0.3 Mpc (Fig. 7). In addition to being perfectly self-consistent with the average of the individual distances, the accuracy of this fit is extremely high; the 1σ uncertainty is less than 2% and illustrates the power of the method when a large sample of bright PN is available.

The ordinates of Figures 5 and 7 represents the luminosity specific stellar death rate, as reflected by $\alpha_{2.5}$, the normalized number of planetaries within 2.5 mag of the PNLF bright end

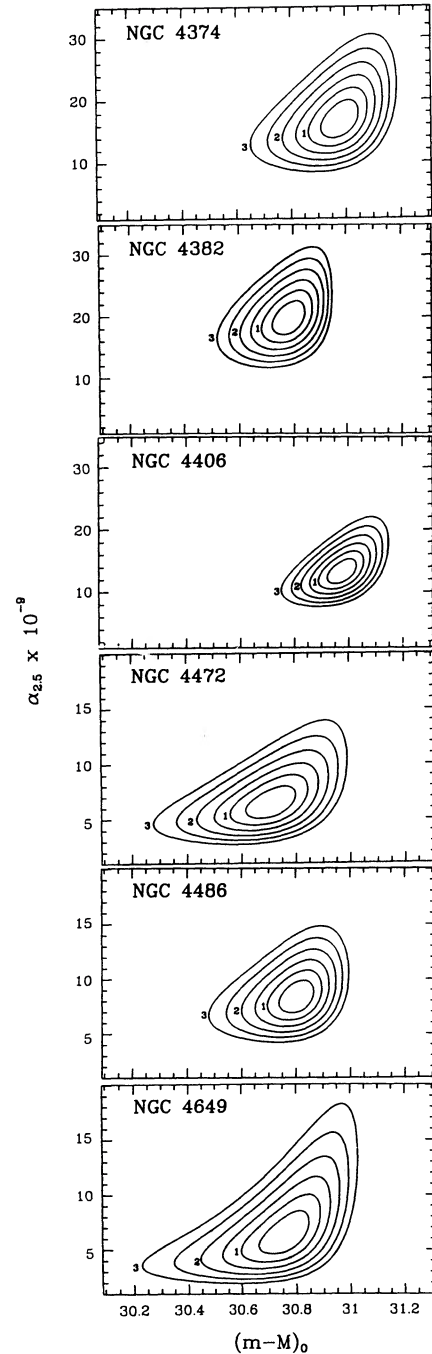


FIG. 5.—Maximum likelihood confidence contours for the six Virgo galaxies derived from fitting the empirical PNLF (convolved with the photometric error function) to the homogeneous and complete samples of PN in each galaxy. The abscissa is the true distance modulus; the ordinate is the number of PN within 2.5 mag of the magnitude cutoff, normalized to the amount of bolometric luminosity surveyed. A differential extinction of $E(B-V) = 0.017$ has been assumed. The contours of probability (shown at intervals of 0.5σ) arise from the uncertainty in fitting the model PNLF to the observed PNLF: horizontal errors reflect the uncertainty in fitting the distance modulus, whereas vertical errors are caused by uncertainties in normalizing to the observed number of PN. The luminosity specific PN density for NGC 4382 is only approximate, since the luminosity contours of that galaxy are irregular.

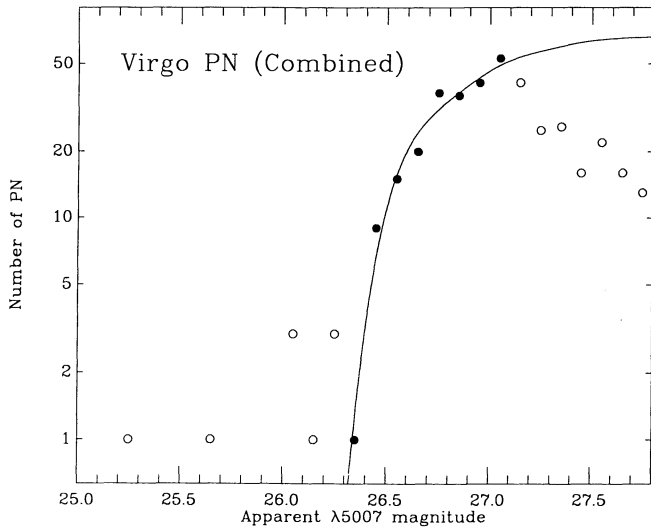


FIG. 6.—The combined PNLF of the six Virgo cluster galaxies, excluding those objects outside the regions of completeness. The PNLF of each galaxy was shifted to the mean distance of 14.7 Mpc prior to inclusion. The solid curve is the model PNLF, as in Fig. 4. The open circles show overluminous objects and PN fainter than the completeness limit and have not been fitted.

cutoff. The most probable values for $\alpha_{2.5}$, and their formal errors, are given in Table 11. All are within a factor of 2 of $\sim 10 \times 10^{-9}$, in good agreement with the values found for M31 (11×10^{-9}) and M81 (16×10^{-9}), but somewhat smaller than that estimated for the Leo Group galaxies ($21\text{--}38 \times 10^{-9}$). When converted to specific stellar death rates, these PN densities translate to values around 5×10^{-12} stars $\text{yr}^{-1} L_{\odot}^{-1}$, a factor of 4 smaller than the theoretical value of Renzini and Buzzoni (1986). Considering the extrapolations and uncertainties involved, this is very good agreement.

e) Error Estimates

The goal of this paper was to derive an *accurate* distance to the Virgo Cluster. In order to assess the success of this study, we now review the errors contributing to the cumulative uncer-

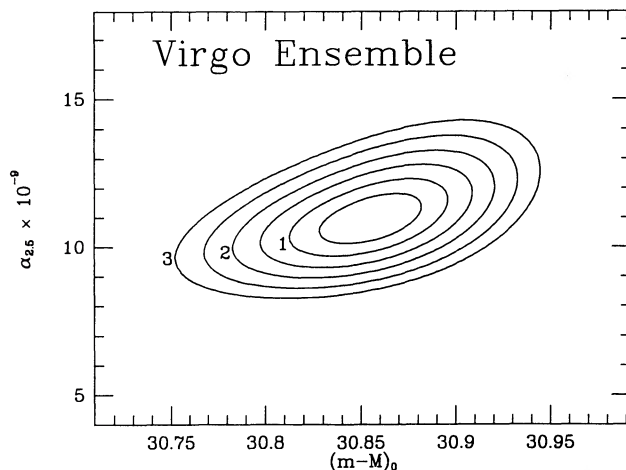


FIG. 7.—The maximum likelihood probability contours for the 233 PN in the statistical sample shown in Fig. 6. Note the extreme precision to which the centroid of the contours can be determined. The 1σ uncertainty of the fit is only 0.04 mag in the distance modulus, which corresponds to an uncertainty of $\pm 2\%$ in the distance.

TABLE 13
SUMMARY OF UNCERTAINTIES

Source	Estimated Error (mags)
Possible systematic	
Distance to M31	0.10
Definition of model PNLF	0.05
Foreground extinction	0.02
Random contributions	
Fit to observed PNLF	0.10
Photometric zero point	0.05
Filter calibration	0.04
Net systematic error	0.13
Net random error	0.05
Net uncertainty	0.14

tainty in our derived distance. Table 13 summarizes the principal error sources we are able to identify; these are classified as either “possible systematic” or “random.” Of course, we are not aware that any of the error sources listed as systematic are actually present. By definition, systematic errors can be removed if they can be identified. It is only when a systematic error cannot be identified that a real error is introduced. In this category we include the uncertainty in distance to our zero-point calibration galaxy, M31, the uncertainty in the functional form of the model PNLF (which is based on observations of 104 PN in that galaxy), and the uncertainty in our estimate for the foreground extinction.

Another potential source of systematic error is that the PNLF in the bulge of M31 may not represent the PNLF properly in the outer regions of Virgo early-type galaxies. For example, the metallicity or age of a stellar population may affect the zero point of its PN luminosity distribution (but not its shape: the data in M31, M81, and the Leo Group galaxies are all consistent with a single form for the PNLF). However, we find no evidence in the Virgo data, or the data from Leo (Paper IV) that variations in the properties of early-type galaxies enter into the distance determination. Figure 8 demonstrates this fact by comparing our PNLF-derived distances with galaxy color, metallicity, and UV flux. From the figure, it is obvious that there is no correlation of any of the quantities with distance. This lack of correlation, we feel, proves the insensitivity of the PNLF to galaxy properties and justifies the use of M31 bulge planetaries as the primary calibrator. Thus we do not include this potential source of error in Table 13.

Extinction internal to M31 may also introduce a systematic error in our distances to other galaxies. In Papers II and III we described a test for that possibility in which we removed from the statistical sample any PN that fall at sky positions coincident with dust lanes. The tests showed that the PNLFs in M31 and M81 were not altered when those objects were discarded, indicating that the bright PN in the bulges of M31 and M81 were unaffected by internal extinction.

Among the random errors, we list the 1σ errors from the fits of the PNLFs using the maximum likelihood method, the photometric zero-point error arising from the standard star solutions and aperture corrections within the individual frames, and the uncertainty in calibrating the narrow-band filter in the converging beams of the telescopes. The entry in Table 13 for net random error includes the adjustment for the six independent measurements.

After combining all error sources in the usual way (see, for example, Bevington 1969), we find that the total uncertainty in

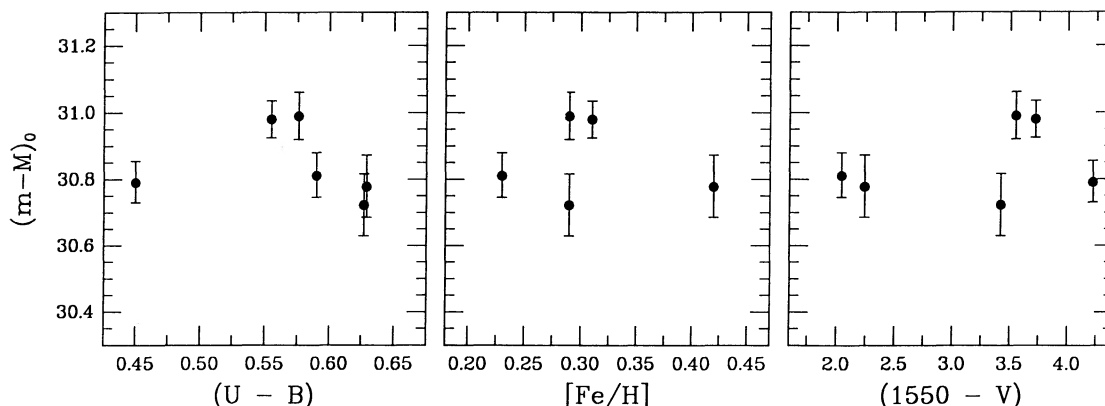


FIG. 8.—A plot of the PNLF based distances as a function of galaxy color (*left*), metallicity (*center*), and ultraviolet color (*right*). Optical colors are from Poulain (1988) and Michard (1982), metallicities are based on the Terlevich *et al.* (1981) calibration of Mg_2 data by Davies *et al.* (1987), and the ultraviolet colors are from Burstein *et al.* (1988). No correlation is seen, indicating that the PNLFs are unaffected by these galaxy properties.

our distance to Virgo is 0.14 mag, or 7%. We believe that this is at least as accurate as any other distance determination for this cluster of galaxies.

V. DISCUSSION

a) The Distance to Virgo

Table 14 compares our derived distance to Virgo of 14.7 ± 1.0 Mpc (error of the mean from Table 13) with other recent results. The factor of 2 in derived distances, extending from 12 Mpc to 22 Mpc, underscores the problem we have attempted to resolve with this study and indicates the need for better error estimates in this field. The recent reviews by Rowan-Robinson (1988) Tammann (1988), and van den Bergh (1989) discuss many aspects of this situation.

Two of the results listed in Table 14 deserve further discussion because they represent results from new or innovative methods. The method of luminosity fluctuations (Tonry, Ajhar, and Luppino 1989), a recently devised technique applicable to early-type galaxies, yields results which are in very good agree-

ment with our own (13.9 ± 1.2 Mpc for their sample of five Virgo galaxies). For the two galaxies we have in common (NGC 4472 and NGC 4406), they find a distance of 15.2 ± 0.6 Mpc, which is essentially identical to our result of 14.8 ± 1.3 Mpc. An earlier study by Tonry and Schneider (1988) which used the same method for NGC 3379 in the Leo Group, yielded an identical distance to the value we presented in Paper IV. This method therefore offers considerable promise as another distance indicator for old stellar populations.

Pierce (1989) recently calibrated the $L-\sigma-\Sigma$ (luminosity-velocity dispersion-surface brightness) relation using our PNLF distance to the Leo Group (Paper IV) as a zero point. Previously, firm distances for early-type galaxies were unavailable, and so the relation was uncalibrated. When we use the I -band relation (which has the smallest dispersion) for the five galaxies we have in common with his survey (NGC 4382 was not included), we derive a distance of 15.0 ± 1.6 Mpc. This is in excellent agreement with the PNLF average of 14.8 ± 0.9 Mpc for the same five galaxies, indicating superb internal consistency for both methods.

We feel that it is appropriate to discuss the methods adopted by the leading representative in Table 14 of the longer distance determinations (Tammann 1988). He concluded that the distance to Virgo is 22.2 ± 0.9 Mpc based on five distance indicators: novae, the Tully-Fisher relation, the $D_n - \sigma$ relation, globular clusters, and supernovae. Of these methods, novae yield the least significant result because the observational task is so difficult (Pritchett and van den Bergh 1987). While the Tully-Fisher relation offers generally good accuracy, it applies only to late-type galaxies and so some interpretation is required to relate the result to the distance of the cluster core. Furthermore, the results published by different groups (cf. Sandage and Tammann 1984; Aaronson *et al.* 1986; Pierce and Tully 1988; Kraan-Korteweg, Cameron, and Tammann 1988; Fouqué *et al.* 1990) are inconsistent. Aaronson *et al.* (1986) attribute this disagreement to the choice of calibrator galaxies, Fouqué *et al.* (1990) present evidence that the differences arise when selecting values for the observational parameters, and Sandage (1988) argues that systematic biases are at fault.

The $D_n - \sigma$ relation was calibrated by Dressler (1987) using the bulges of Sb galaxies for application to the S0 galaxies of Virgo. The scatter in this relation is ~ 0.3 mag, and some galaxies (e.g., NGC 4417) exhibit dramatic deviations. When the relation is calibrated using the Leo Group ellipticals, NGC

TABLE 14
RECENT VIRGO DISTANCE ESTIMATES

Method	Distance (Mpc)	Distance Modulus
Mean of six methods for early-type galaxies (de Vaucouleurs 1985)	11.9 ± 0.6	30.37
Luminosity fluctuations (Tonry, Ajhar, and Luppino 1989)	13.9 ± 1.2	30.72
$L-\sigma-\Sigma$ relation (Pierce 1989)	14.4 ± 1.6	30.79
IR Tully-Fisher relation (Aaronson <i>et al.</i> 1986)	14.6 ± 0.8	30.82
H II region luminosities (Melnick, Terlevich, and Moles 1988)	15.1 ± 1.0	30.89
Optical Tully-Fisher relation (Pierce and Tully 1988)	15.6 ± 1.5	30.97
Optical Tully-Fisher relation (Fouqué <i>et al.</i> 1990)	19.1 ± 1.8	31.41
Novae (Pritchett and van den Bergh 1987)	19.5 ± 3.9	31.45
IR Tully-Fisher relation (Sandage and Tammann 1984)	19.7 ± 3.1	31.47
Type I supernovae (Sandage and Tammann 1982)	21.7 ± 3.1	31.68
Globular cluster luminosity function (Harris 1988)	21.9 ± 2.2	31.70
Mean of five methods (Tammann 1988)	22.2 ± 2.4	31.73
This paper	14.7 ± 1.0	30.84

3377 (E6) and NGC 3379 (E0), the data from Faber *et al.* (1989) give a distance of 16.9 ± 3.1 Mpc to the five Virgo galaxies with both PN and $D_n - \sigma$ measurements (data for NGC 4382 are not available). However, as noted by Ciardullo and Jacoby (1989), the velocity dispersions rise sharply at the centers of some of these galaxies (NGC 4486 and NGC 4649, for example); when this effect is removed by using a velocity dispersion measured a few arcsec away from the nucleus, the derived distance to Virgo becomes 14.5 ± 1.8 Mpc. Thus, this relation appears to be in good agreement with the PNLF method when calibrated with early-type galaxies.

The Virgo globular cluster distance of 21.9 ± 2.2 Mpc (Harris 1988) is based on matching the peaks in the globular cluster luminosity function (GCLF) of target elliptical galaxies in Virgo with the GCLF of the Milky Way, an Sbc galaxy (de Vaucouleurs and Pence 1978; van der Kruit 1984). (If the GCLF of M31, type Sb, is adopted as the reference, the distance to Virgo is reduced by only 7%.) A similar procedure was attempted for the Leo Group galaxy NGC 3379 (Pritchett and van den Bergh 1985) and produced a distance of 6.8 ± 0.8 Mpc, in contrast to the distances of 9.8 Mpc found from the PNLF (Paper IV) and 10.0 Mpc derived from the Tully-Fisher relation for the cluster (Tully and Pierce 1989). Note, however, that the GCLF for NGC 3379 is probably too sparse for an accurate estimate of its peak. The GCLF and the PNLF methods thus far do not agree, and the sense of the disagreement is not consistent.

Supernovae of Type Ia have been observed in three of the galaxies in our sample (NGC 4374, 4382, and 4486). Tammann's (1988) calibration yields an average distance to these galaxies of 20.7 ± 2.4 Mpc, or 20.1 ± 2.3 Mpc if our adopted foreground extinction is applied. The mean PNLF-based distance for the same three is 14.9 ± 0.7 Mpc, in apparent disagreement with this result. However, the calibration of the supernova luminosity given by Tammann (1986) carries an uncertainty of 0.4 mag, and suggests that the two distances are not so disparate after all. The major problem lies in setting the zero-point for use with elliptical galaxies. The primary calibrator, IC 4182 (Branch 1984), is a late-type spiral whose distance (Sandage and Tammann 1982) is based on the measurement of red supergiants. Since the use of this distance indicator is complicated by uncertain corrections for internal extinction (cf. Sandage and Tammann 1982; Humphreys *et al.* 1986), we believe that the uncertainty of 0.2 mag in the distance to Virgo derived from supernovae may be optimistic.

In summary, our PNLF results appear to be in good or excellent agreement with many, but not all, recent distance estimators. The most notable exception is the distance based on supernovae, but even this discrepancy is within the bounds of the errors.

b) *The Depth of the Cluster*

Our derived distances span a range of nearly 2 Mpc, extending from 13.9 to 15.8 Mpc, and the dispersion about the mean of the sample of six galaxies is 0.8 Mpc. After removing the observational uncertainty of ~ 0.5 Mpc (see Table 1), and assuming that the distances to the six galaxies sample a normal distribution, we calculate that the 2σ depth of the cluster core is between 0.9 and 1.8 Mpc at the 68% confidence level, or between 0.7 and 2.9 Mpc at the 95% confidence level. The most probable depth is 1.2 Mpc.

At the derived distance of 14.7 Mpc, the angular extent of the "core" region of the cluster, $\sim 6^\circ$ in radius (Huchra 1985),

corresponds to 3.1 Mpc. This diameter is marginally consistent with the cluster core being spherical. In any case, we are led to conclude that the Virgo core has a depth which is less than 3 Mpc, and probably less than 2 Mpc.

c) *Overluminous Emission-Line Objects*

As noted in § IVa, we found 11 objects with luminosities more than 0.1 mag brighter than expected from the PNLF. Since we did not take H α frames to detect low-excitation objects (except for one field in M87), it is possible that some of these objects are H II regions. However, because all our program galaxies have Hubble types of either E or S0, H II regions are not expected, especially in the galaxy halos. A better explanation, at least for some of the objects just a few tenths of a magnitude brighter than the upper luminosity limit, is that these overluminous PN are the result of optical doubling in which two PN are projected along the line of sight.

We have used two ways to estimate the probability that optical doubling, or merging, will occur. First, using an empirical approach, we took the observed spatial distribution of PN in the bulge of M81 at a distance of 3.5 Mpc (Paper III), and reduced the spatial scale by a factor of 4. We then counted all PN groupings having separations less than 1", a typical seeing diameter. Based on these data, the probability that a PN candidate in Virgo is actually a merger of two or more single candidates is $\sim 5\%$. However, none of the mergers in the M81 data produced a candidate brighter than the most luminous single PN. This suggests that, although ~ 24 of the 486 PN candidates found in Virgo could be the result of optical mergers, none of the overluminous objects is likely to be among this group.

This estimate, however, is not directly applicable to Virgo because the M81 data extended only 2' away from the nucleus. If placed at the distance of Virgo, this radius corresponds to 0.5" and would lead to an overestimate of the merger rate; any PN this close to the nucleus would have been excluded from our statistical samples. In addition, the surface brightness profile of M81 is very different from that of a giant elliptical galaxy, and so the PN distribution in M81 cannot be applied to the Virgo galaxies.

To estimate the probability of mergers at larger galactic radii, we approached the problem from a more theoretical viewpoint. Observations in M31, M81, the Leo Group, and now in Virgo demonstrate that the luminosity specific PN number density is approximately the same (to within a factor of ~ 2) in all early-type galaxies. This is in accordance with the theory of stellar energy production (Renzini and Buzzoni 1986). This being the case, the number density of PN at any point in a galaxy can be predicted directly from the observed surface brightness. It is therefore a straightforward task to model the PN distribution with a Monte Carlo simulation, distributing the PN as the light and following the luminosity law prescribed by the PNLF. Once this is done, the galaxy can be placed at any distance and the number of mergers versus radius computed as in the empirical calculation above. In this manner, the effect of mergers on the PNLF can be quantitatively understood.

Figure 9 shows the results of such a calculation. In the simulation, a set of E0 galaxies similar to NGC 3379 in their surface brightness profiles (de Vaucouleurs and Capaccioli 1979) were placed at a distance of 15 Mpc and the expected PNLFs exterior to several galactic radii were calculated. As demonstrated in the figure, the chance that an optical double will

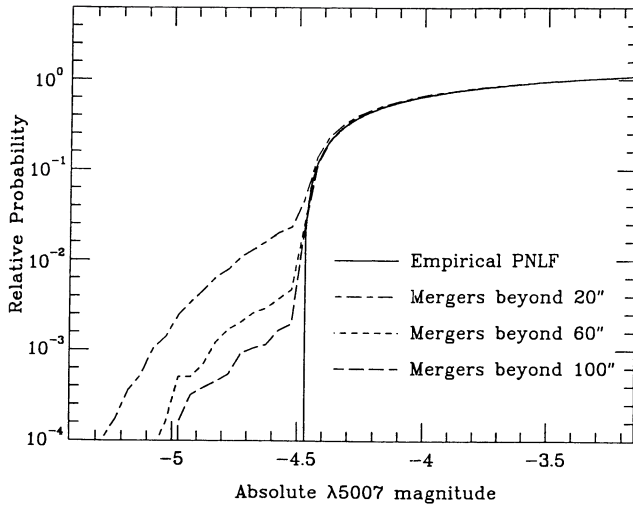


FIG. 9.—The effect of optical merging on the empirical PNLF (solid line) derived from observations exterior to three different radii from the center of a postulated E0 galaxy in Virgo. The PNLF represents the probability of seeing PN at a given magnitude. Beyond radii of 60", the probability becomes small, but nonnegligible, that an overly luminous PN candidate will be seen as the result of a merger.

create an overluminous PN in the halo of a galaxy is small. However, when PN are sampled at galactic radii less than $\sim 20''$, the probability of mergers increases dramatically, and a significant distortion of the PNLF occurs. Although the amplitude of this effect is extremely sensitive to seeing, the trend is clear: optical doubling can effect the PNLF in areas of high surface brightness.

The PN observed in Virgo are typically at $r > 75''$ and at this radius, the chance that an anomalously bright object is the result of an optical merger is only $\sim 0.4\%$. Over a sample of 486 candidates, about two overluminous objects might be identified. Considering the small numbers involved and the uncertainty in the PN production rate and our model for the seeing, it is possible that a few of the superbright candidates could be the result of optical mergers. However, the bulk of the overluminous [O III] sources probably cannot be explained in this way.

The two brightest [O III] sources in our survey (located in NGC 4382 and NGC 4486) that are overluminous by 1.1 and 0.7 mag from the nominal PNLF cutoff are not the result of optical doubling. The object in NGC 4382 is especially noteworthy since it is far from the galaxy nucleus, and there is no evidence for extended emission which might signal an H II complex or star formation. It is possible that the object is a supernova remnant, but this is unlikely—in the absence of an appreciable interstellar medium, an unimpeded expanding supernova shell should adiabatically cool below detectability in just a few years. (NGC 4382 does have a recorded supernova, SN 1960 R, but its position does not coincide with this superbright PN.) It may be worth noting that NGC 4382 is classified as a peculiar galaxy (Sandage and Tammann 1981b) due to the presence of dust patches. We also found faint diffuse emission near the nucleus in our [O III] difference picture; however, the overluminous object is situated well away from these features and so it is not likely to be related to a young population.

The overluminous object in NGC 4486 is similarly perplexing. This galaxy is well known for its unusual features.

Again, the [O III] bright object is well away from any of the commonly seen disturbances (e.g., jet, counterjet), and, interestingly, the object is not seen on an H α image of the region, indicating that it has a very high excitation. Furthermore, a spectrum of this object (which is too faint for any but the bright lines of [O III] $\lambda\lambda 4959, 5007$ to be seen) shows that the object is at the velocity of NGC 4486, and has a single velocity component. Thus it is not likely to be a double. It is possible that this object and the one in NGC 4382 represent some highly unusual emission-line object that would not be seen in surveys of less luminous galaxies. Note that for these two objects to be normal PN, their core masses must be greater than 0.72 and 0.83 M_{\odot} (cf. Fig. 5 of Paper I), which corresponds to progenitor masses of greater than 3–4 M_{\odot} (Kwok 1983).

The conclusion we reached in Paper IV, that the brightest PN candidate is suitable for a distance determination, now appears to be at risk. Should that candidate be overluminous in $\lambda 5007$, then an underestimate of the true distance would be derived. Unfortunately, this estimate cannot be used to derive a lower limit to the distance either: if the brightest candidate is not overly luminous, it may have an intrinsic luminosity that is lower than the upper limit for normal PN candidates, and so an overestimate of the distance would follow. We feel that a reliable distance can be derived only when the luminosity function is used.

d) The Hubble Constant

The Hubble constant follows directly from the distance to Virgo and the heliocentric velocity of the Virgo Cluster corrected to the center of the Local Group and corrected for Local Group infall. A discussion of the extreme range of values for this velocity, V_H , was given by Huchra (1988) who finds that $1227 < V_H < 1597 \text{ km s}^{-1}$, although Gudehus (1989) derives a value of $955 \pm 31 \text{ km s}^{-1}$. The most frequent estimates for this velocity, however, fall between $1187 \pm 73 \text{ km s}^{-1}$ (Kraan-Korteweg 1985) and $1385 \pm 45 \text{ km s}^{-1}$ (Aaronson *et al.* 1986). When combined with our distance to Virgo, $14.7 \pm 1.0 \text{ Mpc}$ (error of the mean), the latter velocities imply values for the Hubble constant between $81 \pm 6 \text{ km s}^{-1} \text{ Mpc}^{-1}$ and $94 \pm 6 \text{ km s}^{-1} \text{ Mpc}^{-1}$ (error of the mean).

To reduce the uncertainty contained in the cluster velocity, the PNLF-based distance to Virgo may be used to calibrate other indicators, such as the $D_n - \sigma$ or $L - \sigma - \Sigma$ relations which may, in turn, be applied to more distant clusters. Because Pierce (1989) derived a distance to Virgo that is statistically indistinguishable from the one presented here, the Hubble constant he obtained using Coma ($88 \text{ km s}^{-1} \text{ Mpc}^{-1}$) would not change significantly if the $L - \sigma - \Sigma$ relation were recalibrated by adding these six Virgo galaxies to the two Leo Group calibrators. We conclude that the Hubble constant is most probably between 75 and $100 \text{ km s}^{-1} \text{ Mpc}^{-1}$, implying a relatively young age for the universe under the assumption of a zero cosmological constant.

VI. CONCLUSION

In this series of five papers, we have demonstrated the use of the PNLF in deriving accurate distances to early-type galaxies. The superb internal consistency of the results presented in this paper and in Paper IV is unparalleled among standard candles for early-type galaxies and strongly supports our position that properties of the parent galaxy have little effect on the derived distances.

We have derived a distance to the core of the Virgo cluster of 14.7 ± 1.0 Mpc, a value in very good agreement with several, but not all, recent determinations. This distance implies that the Hubble constant is between 75 and 100 km s⁻¹ Mpc⁻¹, where the large range in the values is dominated by the uncertainty in the cluster velocity.

The accuracy of the method allows, for the first time, investigations of the three-dimensional spatial structure of a cluster of galaxies. In this study, we found that the core of the Virgo Cluster has a depth which is less than 2 Mpc. In the future we will be able to combine distance determinations based on the PNLF with galaxy velocity measurements and measurements

of individual galaxy masses made using PN as test particles, to map the mass distribution of a galaxy cluster.

We wish to thank the Director of the Canada-France-Hawaii Telescope for granting us observing time. We are also grateful to John Booth for helping with the data reduction during the early phases of this project, to Lindsey Davis for assistance with the surface brightness measurements, and to Sidney van den Bergh for his enthusiastic encouragement in this project. We also wish to thank the anonymous referee of Papers III and IV for suggestions regarding optical merging.

REFERENCES

- Aaronson, M., Bothun, G., Mould, J. R., Huchra, J. P., Schommer, R. A., and Cornell, M. E. 1986, *Ap. J.*, **302**, 536.
- Bevington, P. R. 1969, *Data Reduction and Error Analysis for the Physical Sciences* (New York: McGraw Hill), p. 56.
- Binggeli, B., Tammann, G. A., and Sandage, A. 1987, *A.J.*, **94**, 251.
- Bottinelli, L., Gouguenheim, L., Paturel, G., and Teerikorpi, P. 1986, *Astr. Ap.*, **156**, 157.
- Branch, D. 1984, in *Supernovae as Distance Indicators*, ed. N. Bartel (Berlin: Springer), p. 138.
- Burstein, D., Bertola, F., Buson, L. M., Faber, S. M., and Lauer, T. D. 1988, *Ap. J.*, **328**, 440.
- Burstein, D., and Heiles, C. 1982, *A.J.*, **87**, 1165.
- . 1984, *Ap. J. Suppl.*, **54**, 33.
- Burstein, D., and McDonald, L. H. 1975, *A.J.*, **80**, 17.
- Cawson, M. 1983, Ph.D. thesis, Cambridge University.
- Ciardullo, R., Ford, H. C., Neill, J. D., Jacoby, G. H., and Shafter, A. W. 1987, *Ap. J.*, **318**, 520.
- Ciardullo, R., and Jacoby, G. H. 1989, *Bull. AAS*, **21**, 771.
- Ciardullo, R., Jacoby, G. H., and Bond, H. E. 1989, *A.J.*, **98**, 1648.
- Ciardullo, R., Jacoby, G. H., and Ford, H. C. 1989, *Ap. J.*, **344**, 715 (Paper IV).
- Ciardullo, R., Jacoby, G. H., Ford, H. C., and Neill, J. D. 1989, *Ap. J.*, **339**, 53 (Paper II).
- Cohen, J. G. 1986, *A.J.*, **92**, 1039.
- Davies, R. L. 1981, *M.N.R.A.S.*, **194**, 879.
- Davies, R. L., Burstein, D., Dressler, A., Faber, S. M., Lynden-Bell, D., Terlevich, R. J., and Wegner, G. 1987, *Ap. J. Suppl.*, **64**, 581.
- de Vaucouleurs, G. 1961, *Ap. J. Suppl.*, **6**, 213.
- . 1985, in *ESO Workshop on The Virgo Cluster of Galaxies*, ed. O.-G. Richter and B. Binggeli (Garching: ESO), p. 413.
- de Vaucouleurs, G., and Capaccioli, M. 1979, *Ap. J. Suppl.*, **40**, 699.
- de Vaucouleurs, G., de Vaucouleurs, A., and Corwin, H. G., Jr. 1976, *Second Reference Catalogue of Bright Galaxies* (Austin: University of Texas Press) (RC2).
- de Vaucouleurs, G., and Pence, W. D. 1978, *A.J.*, **83**, 1163.
- Djorgovski, S. 1985, Ph.D. thesis, University of California.
- Dressler, A. 1987, *Ap. J.*, **317**, 1.
- Faber, S. M., Wegner, G., Burstein, D., Davies, R. L., Dressler, A., Lynden-Bell, D., and Terlevich, R. J. 1989, *Ap. J. Suppl.*, **69**, 763.
- Fouqué, P., Bottinelli, L., Gouguenheim, L., and Paturel, G. 1990, *Ap. J.*, **349**, 1.
- Franx, M., Illingworth, G., and Heckman, T. 1989, *Ap. J.*, **344**, 613.
- Frogel, J. A., Persson, S. E., Aaronson, M., and Matthews, K. 1978, *Ap. J.*, **220**, 75.
- Gudehus, D. H. 1989, *Ap. J.*, **342**, 617.
- Harris, W. E. 1988, in *The Extragalactic Distance Scale*, ed. S. van den Bergh and C. J. Pritchet (*A.S.P. Conf. Ser. No. 4*), (Provo: Brigham Young University Press), p. 231.
- Hubble, E., and Humason, M. L. 1931, *Ap. J.*, **74**, 43.
- Huchra, J. P. 1985, in *ESO Workshop on the Virgo Cluster of Galaxies*, ed. O.-G. Richter and B. Binggeli (Garching: European Southern Observatory), p. 181.
- . 1988, in *The Extragalactic Distance Scale*, ed. S. van den Bergh and C. J. Pritchet (*A.S.P. Conf. Ser. No. 4*), (Provo: Brigham Young University Press), p. 257.
- Humphreys, R. M., Aaronson, M., Lebofsky, M., McAlary, C. W., Strom, S. E., and Capps, R. W. 1986, *A.J.*, **91**, 808.
- Jacoby, G. H. 1989, *Ap. J.*, **339**, 39 (Paper I).
- Jacoby, G. H., Ciardullo, R., Ford, H. C., and Booth, J. 1989, *Ap. J.*, **344**, 704 (Paper III).
- Jacoby, G. H., Quigley, R. J., and Africano, J. L. 1987, *Pub. A.S.P.*, **99**, 672.
- Jedrzejewski, R. I. 1987, *M.N.R.A.S.*, **226**, 747.
- Kraan-Korteweg, R. C. 1985, in *ESO Workshop on the Virgo Cluster of Galaxies*, ed. O.-G. Richter and B. Binggeli (Garching: European Southern Observatory), p. 397.
- Kraan-Korteweg, R. C., Cameron, L. M., and Tammann, G. A. 1988, *Ap. J.*, **331**, 620.
- Kwok, S. 1983, in *IAU Symposium 103, Planetary Nebulae*, ed. D. R. Flower (Dordrecht: Reidel), p. 293.
- Landolt, A. U. 1973, *A.J.*, **78**, 959.
- . 1983, *A.J.*, **88**, 439.
- Lauer, T. R. 1985, *Ap. J. Suppl.*, **57**, 473.
- Melnick, J., Terlevich, R., and Moles, M. 1988, *M.N.R.A.S.*, **235**, 297.
- Michard, R. 1982, *Astr. Ap. Suppl.*, **49**, 591.
- . 1985, *Astr. Ap. Suppl.*, **59**, 205.
- Oke, J. B. 1974, *Ap. J. Suppl.*, **27**, 21.
- Pierce, M. J. 1989, *Ap. J. (Letters)*, **344**, L57.
- Pierce, M. J., and Tully, R. B. 1988, *Ap. J.*, **330**, 579.
- Poulain, P. 1988, *Astr. Ap. Suppl.*, **72**, 215.
- Pritchet, C. J., and van den Bergh, S. 1985, *A.J.*, **90**, 2027.
- . 1987, *Ap. J.*, **318**, 507.
- Renzini, A., and Buzzoni, A. 1986, in *Spectral Evolution of Galaxies*, ed. C. Chiosi and A. Renzini (Dordrecht: Reidel), p. 195.
- Rowan-Robinson, M. 1988, *Space Sci. Rev.*, **48**, 1.
- Sandage, A. 1973, *Ap. J.*, **183**, 711.
- . 1988, *Ap. J.*, **331**, 605.
- Sandage, A., and Tammann, G. A. 1981a, in *Astrophysical Cosmology*, ed. H. A. Brück, G. V. Coyne, and M. S. Longair (Vatican: Pontificia Academia Scientiarum), p. 23.
- . 1981b, *A Revised Shapley-Ames Catalog of Bright Galaxies* (Washington: Carnegie Institute of Washington).
- . 1982, *Ap. J.*, **256**, 339.
- . 1984, *Nature*, **307**, 326.
- Sargent, W. L. M., Young, P. J., Bokserberg, A., Shortridge, K., Lynds, C. R., and Hartwick, F. D. A. 1978, *Ap. J.*, **221**, 731.
- Seaton, M. J. 1979, *M.N.R.A.S.*, **187**, 73p.
- Shapley, H., and Ames, A. 1926, *Harvard Circ.*, No. 294.
- Stetson, P. 1987, *Pub. A.S.P.*, **99**, 191.
- Stone, R. P. S. 1977, *Ap. J.*, **218**, 767.
- Tammann, G. A. 1986, in *IAU Symposium 124, Observational Cosmology*, ed. A. Hewitt, G. R. Burbidge, and L. Z. Fang (Dordrecht: Reidel), p. 151.
- . 1988, in *The Extragalactic Distance Scale*, ed. S. van den Bergh and C. J. Pritchet (*A.S.P. Conf. Ser. No. 4*), (Provo: Brigham Young University Press), p. 282.
- Terlevich, R., Davies, R. L., Faber, S. M., and Burstein, D. 1981, *M.N.R.A.S.*, **196**, 381.
- Tonry, J. L., Ajhar, E. A., and Luppino, G. A. 1989, *Ap. J. (Letters)*, **346**, L57.
- Tonry, J., and Schneider, D. P. 1988, *A.J.*, **96**, 807.
- Tully, B., and Pierce, M. 1989, private communication.
- van den Bergh, S. 1989, in *Astr. Ap. Rev.*, **1**, 111.
- van der Kruit, P. C. 1984, *Astr. Ap.*, **140**, 470.
- Whitmore, B. C., McElroy, D. B., and Tonry, J. L. 1985, *Ap. J. Suppl.*, **59**, 1.

ROBIN CIARDULLO and GEORGE H. JACOBY: Kitt Peak National Observatory, P.O. Box 26732, Tucson, AZ 85726

HOLLAND C. FORD: Space Telescope Science Institute, 3700 San Martin Drive, Baltimore, MD 21218